AD-A173 448

Calculation of Far Field Radiation and Diffraction Wave Patterns Using the Kochin Function Approach for a Series of Ship Hulls

HENRY T. WANG

Fluid Dynamics Branch
Marine Technology Division

DTIC
ELECTE
OCT 24 1986

B

DTIC FILE COPY

86 10 24 024

AD-A173 448

REPORT DOCUMENTATION PAGE

1a. REPORT SECURITY CLASSIFICATION UNCLASSIFIED		1b. RESTRICTIVE MARKINGS			
2a. SECURITY CLASSIFICATION AUTHORITY		3. DISTRIBUTION/AVAILABILITY OF REPORT Approved for public release; distribution unlimited.			
2b. DECLASSIFICATION/DOWNGRADING SCHEDULE					
4. PERFORMING ORGANIZATION REPORT NUMBER(S) NRL Memorandum Report 5822		5. MONITORING ORGANIZATION REPORT NUMBER(S)			
6a. NAME OF PERFORMING ORGANIZATION Naval Research Laboratory	6b. OFFICE SYMBOL (If applicable) Code 5841	7a. NAME OF MONITORING ORGANIZATION Office of Naval Research			
6c. ADDRESS (City, State, and ZIP Code) Washington, DC 20375-5000		7b. ADDRESS (City, State, and ZIP Code) Arlington, VA 22217			
8a. NAME OF FUNDING/SPONSORING ORGANIZATION Office of Naval Research	8b. OFFICE SYMBOL (If applicable)	9. PROCUREMENT INSTRUMENT IDENTIFICATION NUMBER			

8c. ADDRESS (City, State, and ZIP Code) Arlington, VA 22217	10. SOURCE OF FUNDING NUMBERS			
	PROGRAM ELEMENT NO. 61153N	PROJECT NO.	TASK NO RR023- 01-41	WORK UNIT ACCESSION NO. DN280-006

11. TITLE (Include Security Classification)
Calculation of Far Field Radiation and Diffraction Wave Patterns Using the Kochin Function Approach for a Series of Ship Hulls

12. PERSONAL AUTHOR(S)
Wang, Henry T.

13a. TYPE OF REPORT Interim	13b. TIME COVERED FROM _____ TO _____	14. DATE OF REPORT (Year, Month, Day) 1986 September 30	15. PAGE COUNT 37

16. SUPPLEMENTARY NOTATION

17.	COSATI CODES		18. SUBJECT TERMS (Continue on reverse if necessary and identify by block number)
FIELD	GROUP	SUB-GROUP	Far field waves Radiation and diffraction. Strip theory, Kochin function.

19. ABSTRACT (Continue on reverse if necessary and identify by block number)

The report presents the calculation procedure and numerical results for the far field radiation and diffraction wave patterns around a ship at zero forward speed. The calculation procedure uses the strip-theory Ship Motions Program to obtain the motion transfer coefficients and singularity strengths in the form of the integrated Kochin functions. These results are then combined with an asymptotic expression for the far field wave elevation due to a three-dimensional oscillating source to obtain the ship wave patterns.

The wave patterns are calculated for a series of six ships, including a strut-like hull, excited by ambient waves representative of Sea States 2, 4, 6, and 8. The radiation waves are calculated for all six modes of ship oscillation. The diffraction waves are calculated for wave headings ranging from following seas to head seas. The accuracy of a commonly used long wavelength approximation to the Kochin function in which the singularity distribution over the hull surface is collapsed to a line distribution, is also discussed.

20. DISTRIBUTION/AVAILABILITY OF ABSTRACT ☒ UNCLASSIFIED/UNLIMITED ☐ SAME AS RPT. ☐ DTIC USERS	21. ABSTRACT SECURITY CLASSIFICATION UNCLASSIFIED	
22a. NAME OF RESPONSIBLE INDIVIDUAL Henry T. Wang	22b. TELEPHONE (Include Area Code) (202) 767-2516	22c. OFFICE SYMBOL Code 5841

DD FORM 1473, 84 MAR
83 APR edition may be used until exhausted
All other editions are obsolete

☆U.S. Government Printing Office: 1985—687-047

i

CONTENTS

CALCULATION OF FAR FIELD RADIATION AND DIFFRACTION WAVE PATTERNS USING THE KOCHIN FUNCTION APPROACH FOR A SERIES OF SHIP HULLS

1. INTRODUCTION

The calculation of the force and motion coefficients of a surface ship excited by ambient ocean waves is a problem of widespread interest. The motion coefficients are of interest to ensure the safety and comfort of the crew and passengers, as well as the stability of the onboard cargo. The force coefficients are of interest since they are components of the equations of motion, and also enter in the calculations of the structural behavior of the ship. Practical computational approaches may be broadly classed in two categories: strip theory where interactions between transverse ship sections are neglected, and fully three-dimensional approaches. An example of the strip theory approach is the DTNSRDC Ship Motion Program, SMP [1,2] while an example of the second approach is that by Chang [3]. A comparison of these two approaches for a series of ship hulls has been conducted by Wang and Chang [4].

A related problem of considerable interest is the calculation of the wave profile next to the ship. This is of interest, for example, in deck wetness and slamming calculations. Examples of such calculations are those by Lee [5] and Beck [6].

All of the above are concerned with the near field flow and wave pattern next to the ship hull. While there have been some studies outlining the general calculation procedure for the far field wave pattern [7,8], actual calculations of these waves for typical ship hulls appear to be lacking. This report presents the calculation procedure and numerical results for the far field radiation and diffraction wave pattern for a series of ship hulls at zero forward speed due to typical ocean waves. Radiation waves refer to those caused by the three translational and three rotational oscillatory motions of the ship, while diffraction waves are due to the scattering of the incident exciting wave by the ship hull, taken to be stationary.

The calculation procedure for the near field flow, outlined in [8], is briefly summarized here. The calculation of the far field wave patterns, using the Kochin function approach, is discussed in greater detail. It is shown that the suggested collapse of the hull surface singularities onto a line [7,8] is equivalent to an approximate calculation of the Kochin function, assuming that the length of the exciting wave is much larger than the beam and draft of the ship.

Radiation and diffraction wave patterns are calculated for a series of six ship hulls ranging in

length from 140 to 990 ft, four wavelengths of the exciting waves ranging from 35 to 998 ft, and five wave headings ranging from following to head seas. The wave characteristics are given in terms of figures showing the variation with spatial direction of the amplitude and phase at a given distance from a fixed point on the ship. The figures show typical variations of the wave patterns with characteristics of exciting wave and hull. The accuracy of the calculated waves using the approximate Kochin function procedure, for different wavelengths, is also shown. The report concludes with a summary of the principal findings.

2. DESCRIPTION OF CALCULATION APPROACH

Adopting the usual assumption of linearized potential flow, the problem essentially consists of two parts: the evaluation of the potential flow on and near the ship hull and the extrapolation of this solution to obtain the far field waves. A detailed description of the procedure for calculating the near field flow is given in [8] and hence is only summarized here. The evaluation of the Kochin function and its use in obtaining the far field wave pattern is discussed in greater detail.

2.1 Calculation of Near Field Flow

The near field problem consists of finding a potential function ϕ which satisfies Laplace's equation, the free surface condition, the radiation condition of outward progressive waves at infinity, and the kinematic condition of no flow through the ship hull. In the commonly used Green's function approach, the procedure is to place a series of singularities on the hull surface, which satisfy the first three conditions, and determine their strengths from the kinematic condition on the hull surface. Largely due to the presence of the free surface condition, the general solution of this problem, even with the linearization assumption, is still quite complex.

A considerable simplification results if the beam and draft of the ship, as well as length of the exciting wave are all taken to be small compared to the length of the ship. In this case, longitudinal interactions between ship cross sections may be neglected, and the complex three-dimensional problem reduces to a series of simpler two-dimensional problems for various transverse sections, or strips. An example of this strip theory approach is the Ship Motion Program (SMP) [1,2] developed at DTNSRDC. For the zero speed case considered in the present work, it is shown in [4] that SMP calculates force coefficients which are in fair agreement with those given by a three-dimensional approach [3] and motion coefficients which are in reasonable agreement.

The coordinate system used in the calculations in SMP (and also used in the present work) is shown in Figure 1. The origin lies on the undisturbed free surface, at the longitudinal center of gravity, and in the vertical plane of symmetry. The x-axis is directed forward, the y-axis to port, and the z-axis upwards. In this coordinate system, following and head seas correspond respectively to headings of 0 and 180 degrees. It should be noted that the above coordinate system and sea heading convention do *not* correspond to those used for input and output in SMP.

2

The total unsteady potential ϕ is written as the following sum

$$\phi = [\alpha(\phi_0 + \phi_7) + \sum_{j=1}^{6} \xi_j \phi_j] e^{i\omega t} \tag{1}$$

where α is the amplitude of the incident wave

ϕ_0 is the potential of the incident wave of unit amplitude

ϕ_7 is the diffraction potential

ξ_j is the amplitude of the jth oscillation

ϕ_j is the radiation potential due to the jth oscillation of unit amplitude

ω is the circular frequency.

As shown in Figure 1, $j = 1,3,5$ correspond to the motions of surge, heave, and pitch in the vertical plane, and $j = 2,4,6$ correspond to the lateral motions of sway, roll, and yaw.

The radiation potentials ϕ_j are obtained by placing two-dimensional Havelock sources on a series of transverse cross sections along the ship longitudinal axis. The strengths of these singularities are determined by the kinematic condition of no flow through the hull cross section for each of the oscillation modes, using a procedure originally implemented by Frank [9]. It is shown in [7,8] that the diffraction potential ϕ_7, which is obtained from the kinematic condition of no flow of the incident wave through the stationary ship hull, may be expressed in terms of the heave and sway radiation potentials, as follows

$$\phi_7 = -(\phi_3 - i\sin\beta\,\phi_2)e^{-ikx\cos\beta} \tag{2}$$

where β is the wave heading

$k = \dfrac{\omega^2}{g} = \dfrac{2\pi}{\lambda}$ is the wave number

ω is the circular frequency of the exciting wave

λ is the wavelength of the exciting wave.

2.2 Calculation of Far Field Wave Patterns

To first order, the strengths of the sources obtained for the near field may also be used to obtain the far field waves [7]. However, the sources themselves must be changed from those for two dimensions, G_{2D}, to those for three dimensions, G_{3D}. For example, a two-dimensional source gives far field waves of constant amplitude whereas in three dimensions they decay due to cylindrical spreading.

Three approaches are outlined in [8] for using the near field singularity strengths to obtain the far field waves: by using the damping coefficients, by compressing the hull surface source distribution to a line distribution, or by using the Kochin function which represents an integral over the hull surface of the source strengths weighted by an exponential function. In the present work, the Kochin function approach is taken. It is shown below that the line distribution approach essentially represents a long wavelength approximation of the Kochin function.

In their classic and comprehensive survey of free surface flows, Wehausen and Laitone [10] give the following asymptotic expression for the far field wave elevation ζ_j of the radiation wave due to an oscillation ξ_j of unit amplitude

$$\zeta_j \sim \mathrm{Re}\left[\frac{\omega}{g}\sqrt{\frac{k}{2\pi R}}\,\bar{H}_j(k,\theta)\,e^{i(kR+\omega t-\frac{\pi}{4})}\right]$$

$$= \mathrm{Re}\left[\frac{1}{4\pi}\frac{\omega}{g}\bar{H}_j\left(G^q_{3D}e^{i\omega t}-2\pi\sqrt{\frac{2k}{\pi R}}\,e^{i(kR-\pi/4)}\,e^{i\omega t}\right)\right] \tag{3}$$

where $j = 1,\ldots,6$ denote the six modes of ship oscillation

$R = \sqrt{x^2+y^2}$ denotes the radius in the horizontal plane, measured from the origin shown in Figure 1

$\theta = \tan^{-1}y/x$ is the direction in the horizontal plane, measured from the x-axis

$\bar{H}_j$ is the complex conjugate of the Kochin function H_j

G^q_{3D} is the asymptotic expression for the three-dimensional source potential at large R.

Several equivalent forms for H_j are given in [10]. In the present work, it is of particular interest to consider H_j as the following weighted integral of the singularity strength distribution over the hull surface S

$$H_j(k,\theta) = -\iint_S \gamma_j(\xi,\eta,\zeta)\,e^{[k\zeta+ik(\xi\cos\theta+\eta\sin\theta)]}dS \tag{4}$$

where γ_j is the hull surface distribution of singularity strengths calculated by SMP for the jth mode of ship oscillation. The exponential function precisely accounts for the difference in the wave due to a source located away from the origin. Thus, the factor $e^{k\zeta}$ gives the well known vertical exponential damping of the wavemaking capability of a source situated below the free surface. The factor $e^{ik(\xi\cos\theta+\eta\sin\theta)}$ gives the change in phase of the wave originating at $x=\xi$, $y=\eta$ from that originating at $x=y=0$.

It is of interest to note that the far field asymptotic expression is valid at relatively short distances from a given source. In the two-dimensional case, Marnyanskii [11] shows that at a distance of 0.3 λ

4

from the source, there is little effect of the near field terms. In the three-dimensional case, at a distance of $\lambda/6$ from an oscillating source submerged below the free surface, Liu [12] obtains a difference of approximately 15% in the wave elevations calculated by the far field and complete formulas.

For the actual case where the ship oscillation is not of unit amplitude but is the response to a wave of amplitude α, the resultant wave elevation ζ_{Rj} must be written in terms of α and the transfer function T_j which is a function of wave frequency ω and wave heading β

$$\zeta_{Rj}\ (k,\theta,R,\beta) \sim \mathrm{Re}\left[\alpha T_j(\omega,\beta)\frac{\omega}{g}\sqrt{\frac{k}{2\pi R}}\,\bar{H}_j\ (k,\theta)\ e^{i(kR+\omega t-\pi/4)}\right]$$

$$\sim \mathrm{Re}\ [A_j(k,\theta,R,\beta)\ e^{i(kR+\omega t-\pi/4)}] \tag{5}$$

where $A_j\ (k,\theta,R,\beta) = \alpha T_j\ \dfrac{\omega}{g}\sqrt{\dfrac{k}{2\pi R}}\,\bar{H}_j\ (k,\theta)$ is the amplitude coefficient of ζ_{Rj}. It may be noted that, for the sake of simplicity, the incoming wave is here assumed to have zero phase with respect to the origin.

The formula for the resultant diffraction wave ζ_{R7} is conveniently obtained from Eqs. (2) and (5). Noting that the ship is taken to be stationary and hence T_j does not enter, ζ_{R7} is given by

$$\zeta_{R7} = \zeta_{R7V} + \zeta_{R7L}$$

$$= \mathrm{Re}\left[\alpha\frac{\omega}{g}\sqrt{\frac{k}{2\pi R}}\ (\bar{H}_{7V}(k,\theta,\beta) + \bar{H}_{7L}\ (k,\theta,\beta))\ e^{i(kR+\omega t-\pi/4)}\right]$$

$$= \mathrm{Re}\left[(A_{7V}\ (k,\theta,R,\beta) + A_{7L}\ (k,\theta,R,\beta)e^{i(kR+\omega t-\pi/4)}\right] \tag{6}$$

where $A_{7V} = \alpha\ \dfrac{\omega}{g}\sqrt{\dfrac{k}{2\pi R}}\,\bar{H}_{7V}$ and $A_{7L} = \alpha\ \dfrac{\omega}{g}\sqrt{\dfrac{k}{2\pi R}}\,\bar{H}_{7L}$ are respectively the symmetric (vertical plane) and antisymmetric (lateral plane) components of A_7, and H_{7V} and H_{7L} are evaluated from Eq. (4) with $\gamma_{7V} = -\gamma_3\ e^{-ik\xi\cos\beta}$ and $\gamma_{7L} = i\sin\beta\ \gamma_2\ e^{-ik\xi\cos\beta}$.

2.3 Long Wavelength Approximation of the Kochin Function

It is of interest to investigate the consequence of evaluating the Kochin function by assuming the wavelength λ to be long. In particular, if λ is large compared to the transverse dimensions of beam and draft of the ship, the exponential terms in Eq. (4) may be approximated to first order by

$$e^{k\zeta} \approx 1 + k\zeta \tag{7a}$$

$$e^{ik\eta\sin\theta} = \cos\ (k\eta\sin\theta) + i\sin\ (k\eta\sin\theta)$$

$$\approx 1 + ik\eta\sin\theta. \tag{7b}$$

Considering that γ_j (ξ, η, ζ) is even in η for the vertical modes $(j = 1,3,5)$ and odd in η for the lateral modes $(j=2,4,6)$, the integral (4) for a given transverse section C at $\xi = \xi_0$ takes on the following two forms

$$H_j \approx -\int_C \gamma_j \; (\xi_0, \eta, \zeta) \; (1 + k\zeta) \; (1) \; dl \qquad j = 1,3,5 \tag{8a}$$

$$H_j \approx -ik \; \sin\theta \int_C \gamma_j \; (\xi_0, \eta, \zeta) \; (1 + k\zeta) \; (\eta) \; dl \qquad j = 2,4,6 \tag{8b}$$

If one neglects the wave damping term $1 + k\zeta$, Eqs. (8a) and (8b) reduce to

$$H_j \approx -Q_j \quad j = 1,3,5 \tag{9a}$$

$$H_j \approx -ik\sin\theta \; M_j \quad j = 2,4,6 \tag{9b}$$

where Q_j and M_j are precisely the resultant point source and dipole strengths for a given transverse section C given in [8]. The factor $ik \; \sin\theta$ appearing in Eq. (9b) is accounted for in [8] by considering the dipole M_j to create waves given by the dipole potential $\dfrac{\partial G^q_{3D}}{\partial y}$. Using the definitions given in Eq. (3)

$$\frac{\partial R}{\partial y} = \frac{y}{R} = \sin\theta, \tag{10}$$

from which it follows that at large values of R

$$\frac{\partial}{\partial y} \; G^q_{3D} \sim ik \sin\theta \; G^q_{3D} \tag{11}$$

Thus, the suggested approach of collapsing the section singularity distribution to a single point is equivalent to evaluating the Kochin function for large wavelengths, neglecting in addition the vertical damping term $1 + k\zeta$. In the present work, this term has been retained. It should be noted, however, that while this term may improve the approximation at large values of λ (small values of $|k\zeta|$), it may actually worsen it at intermediate and large values of $|k\zeta|$. For example, for large $|k\zeta|$, $1 + k\zeta$ may become negative while the actual minimum value of $e^{k\zeta}$ is 0.

3. DESCRIPTION OF COMPUTER RUNS

3.1 Choice of Ship Hulls

A total of six ship hulls were considered. The principal geometric characteristics of these hulls are shown in Table 1. The DE1006 destroyer and the CVA-59 carrier were previously investigated in the force and motion coefficient study [4]. Their lengths are respectively 308 and 990 ft. In order to investigate the effect of appendages on the wave pattern, the DE10NA was also selected. It is identical

to the DE1006 with the exception that the appendages are removed. In order to investigate the effect of ship length, shorter geosims of the CVA-59 were also chosen: the CVASH and CVAXS with respective lengths of 308 and 140 ft. Finally, in order to investigate the wavemaking of a strut, which is characterized by a large draft to beam ratio, SHSTNA, the Sharma strut [13] scaled to a length of 308 ft. was also selected.

3.2 Choice of Exciting Waves

The exciting waves were taken to have wavelengths λ of 35.1, 140.4, 315.9, and 998.3 ft. These are typical for Sea States 2, 4, 6, and 8, respectively. Table 2 shows the values of λ, the corresponding values of ω, and typical values of the amplitude α. The three largest values of λ approximate closely the lengths of the various hulls, while the lowest value of λ approximates the beam or draft of most of the hulls. For convenience, the four particular values of λ were selected so that the corresponding values of ω coincide precisely with four of the 30 values for which force and motion coefficients are calculated in SMP.

For each wavelength, five wave headings β were selected: 0, 45, 90, 135, and 180 degrees. These correspond respectively to following, quartering, beam, bow, and head seas. Thus, a total of 20 different exciting waves, in terms of $\lambda-\beta$ combinations, were used for each ship.

3.3 Computer Program SMPRAD

The above matrix of computer runs were made by using computer program SMPRAD. It consists of program SMP to make the near field calculations of source strength $\gamma(\xi,\eta,\zeta)$ as well as the complex motion transfer function T_j. Additional coding was then developed to perform the far field calculations resulting in the complex amplitude coefficients A_j.

4. FAR FIELD WAVE PATTERNS

4.1 Method of Presentation

A number of sample plots are presented to give an indication of the major features of the radiation and diffraction wave patterns. The figures essentially give the phase angle $\psi_j(R_0,k,\theta,\beta)$ and various measures of the magnitude $|A_j(R_0,k,\theta,\beta)|$ of the complex amplitude coefficient A_j defined in Eqs. (5) and (6) at a reference radius $R_0 - 308$ ft. This is equal to the ship length for four of the hulls. Recall that $j - 1, \ldots, 6$ refer to the six radiation waves due to ship oscillation, while $j - 7$ refers to the diffraction wave around a stationary ship.

The value of ψ_j is simply given by

$$\psi_j(k,\theta,\beta) = \tan^{-1}\frac{Re(A_j)}{Im(A_j)} \qquad (12)$$

and is independent of R_0. The value of $|A_j|$ is given by

$$|A_j(k,\theta,\beta)| = \sqrt{(ReA_j)^2 + (Im\,A_j)^2}. \qquad (13)$$

Eqs. (5) and (6) show that the values of $|A_j|$ for different reference distances R_0 and R_1, A_{j0} and A_{j1}, are simply related by

$$\frac{|A_{j0}|}{|A_{j1}|} = \frac{\sqrt{R_1}}{\sqrt{R_0}} \qquad (14)$$

In the following figures, the dimensional wave amplitude $|A_j|$ is given in terms of one of the following dimensionless ratios:

$$A_{j\alpha}(k,\theta,\beta) = \frac{|A_j|}{\alpha} \qquad (15a)$$

$$A_{jb}(k,\theta,\beta) = \frac{|A_j|}{\max_i\{|A_j(k,\theta_i,\beta)|\}} \qquad (15b)$$

$$A_{jc}(k,\theta,\beta) = \frac{|A_j|}{\max_i\{|A_j(k,\theta_i,\beta)|,|A_{j\alpha}(k,\theta_i,\beta)|\}} \qquad (15c)$$

where the subscript a refers to A_j calculated by using the approximate evaluation of H_j given in Eqs. (8). The ratio $A_{j\alpha}$ is simply the amplitude of the radiation or diffraction wave referenced to the amplitude of the exciting wave. This is useful in comparing the relative wavemaking of the ships with respect to different exciting waves. The ratio A_{jb} normalizes $|A_j|$ so that the maximum value is 1. This is useful in comparing the relative shapes of the various wave modes $j = 1,...,6,7$. The ratio A_{jc} is similar to A_{jb} with the exception that it is normalized with respect to A_j using the accurate and long wavelength approximations of H_j. This is useful for ascertaining the error incurred in using the long wavelength approximation of $|A_j|$.

In all cases, the wave patterns are given in terms of the variation of ψ_j and the various measures of $|A_j|$ with the direction θ. All of the curves in these figures are drawn with one of six line styles which are identified as Curves 1 to 6, shown in Figure 2.

8

Figures 3a to 3f show the variation with θ of the dimensionless amplitude coefficient $A_{j\alpha}$ for the radiation waves for the three vertical and the three lateral modes. Figures 4a to 4f show corresponding variations of the phase angle ψ_j. Due to the large values of the lateral mode waves of the strut-shaped SHSTNA hull, their values have been divided by 10 in order to be on the same scale as the other hulls. For the sake of consistency, $A_{j\alpha}$ for the vertical modes as well as the diffraction waves shown in Figure 5 for this hull have also been divided by 10. This fact is clearly indicated in the legend for these figures. The wavelength λ and heading β of the exciting wave considered in each figure correspond to the particular case out of the 20 $\lambda - \beta$ combinations which give the largest value of $A_{j\alpha}$ for the DE1006.

Figures 5a and 5b respectively show the variation of $A_{7V\alpha}$ and $A_{7L\alpha}$, the symmetrical and anti-symmetrical components of the diffraction wave. Figures 6a and 6b show corresponding values for the phase angles ψ_{7V} and ψ_{7L}. The results shown in these figures are for $\lambda = 140.4$ ft and $\beta = 135$ deg, a bow sea. For four of the hulls, this value of λ lies intermediate between the beam and length of the ship, an optimum range of λ for the low order diffraction theory used in this work.

Figures 7a to 7c respectively show the variation of the normalized amplitude A_{jb} of the four vertical modes ($j = 1,3,5,7V$) for $\lambda = 315.9$ ft, $\beta = 135$ deg, for the geosims of different length: CVA-59, CVASH, and CVAXS. Figures 8a to 8c show corresponding results for the four lateral modes ($j = 2,4,6,7L$).

Figures 9a to 9d respectively show the variations of A_{jb} of the vertical modes ($j = 1,3,5,7V$) for different wavelengths λ for the DE1006. Figures 10a to 10d show the corresponding variation of A_{jb} with λ for the lateral modes ($j = 2,4,6,7L$).

Figures 11a and 11b respectively show the variation of the diffraction amplitude coefficients $A_{7V\alpha}$ and $A_{7L\alpha}$ with wave heading β for the previously considered intermediate wavelength $\lambda = 140.4$ ft (see Figs. 5 and 6) for the DE1006.

Figures 12a to 12d respectively show the variation with λ of the exact and approximate values of $A_{j\epsilon}$ of heave, pitch, sway, and yaw at a fixed heading of 90 deg for the DE1006.

4.3 Discussion of Wave Patterns

Leaving aside the unusual strut-shaped hull, SHSTNA, Figure 3a shows the expected trend that the wave amplitudes for surge are one order of magnitude lower than the other radiation modes. The large value for the strut case is that, due to its extremely thin waterplane section, there is little potential damping and motions may be large near resonance with resultant large waves. This also accounts for

the larger values of pitch for the SHSTNA, shown in Figure 3c. Lee [14] discusses the need for adding viscous damping terms to obtain accurate motion predictions near resonance for twin hull ships which have strut-like members. For the lateral modes Figures 3d and 3e show that the wave patterns for the SHSTNA are similar to those of the other hulls, but with maximum values which are an order of magnitude higher. This is due to its large draft. In the case of sway, shown in Figure 3f, the wave amplitudes for the SHSTNA are identically zero since its hull is symmetric fore and aft and the wave heading is 90 deg.

Figure 3 shows that the wave pattern varies significantly with mode and ship length. Thus, $A_{j\alpha}$ for surge and pitch tend to have minimum values at $\theta = 90$ deg while the remaining modes tend to have maximum values here. In both Figures 3 and 4, the curves for the shortest hull CVAXS tend to have the smoothest variation with θ, while those for the longest hull CVA-59 tend to have the sharpest variation. This is simply an indication that a given value of λ is longest relative to the CVAXS and shortest relative to the CVA-59.

Figures 3d to 3f show that the removal of appendages from the DE1006 increases the maximum wave amplitude of the rotational modes of yaw and roll by approximately 20 percent and has relatively little effect on the translational sway mode.

In the case of the diffraction waves, shown in Figures 5 and 6, perhaps the most striking feature is the extremely large values for the CVA-59, which has the longest length. Here, the exciting wave is shortest relative to it, and hence undergoes the largest scattering. By the same reasoning, the CVAXS has the shortest length and the exciting wave undergoes relatively little scattering, resulting in small diffraction wave amplitudes. The effect of hull length is also evident in Figures 6a and 6b, which show that the phase angle variation is sharpest for the CVA-59 and smoothest for the CVAXS.

As in the case for the radiation waves, the behavior of the strut-shaped SHSTNA sharply differs from that of the other hulls of equal length. It has the lowest values for the vertical diffraction wave amplitude, but the second highest (next to the previously mentioned CVA-59 case) lateral diffraction waves. These are again due respectively to its thin beam and deep draft.

Figures 7 and 8 show that the normalized wave amplitudes $A_{j\delta}$ become smoother with increasing ship length for the geosim series CVAXS (140 ft), CVASH (308 ft), and CVA-59 (990 ft). The wave is fixed at $\lambda = 315.9$ ft and $\beta = 135$ deg. The largest change in the wave patterns occurs between the CVAXS and CVASH hulls, and less of a change occurs between the CVASH and CVA-59 hulls. Thus, the shape of the long-wavelength wave pattern is generally established for $\lambda \approx L$.

10

Figures 9 and 10 show the manner in which A_{j8} of each of the eight wave modes approaches the long wavelength pattern for increasing wavelength for the DE1006 hull (308 ft). The modes of surge, pitch, and yaw, which have minima in the beam direction ($\theta = 90$ deg), tend to have more pronounced variations with λ than the remaining modes which have maxima at $\theta = 90$ deg.

Figures 11a and 11b show that the θ - value of the maxima of the dimensionless diffraction wave amplitudes A_{7V_α} and A_{7L_α} for the DE1006 shifts along the θ - axis to always coincide with the wave heading β. The maximum value of the vertical wave A_{7V_α} does not vary with β, but that of the lateral wave A_{7L} varies according to the $\sin\beta$ factor given in Eq. (6). Thus, for following and head seas, $\beta = 0$ and 180 deg, Figure 11b shows the expected case of the absence of lateral diffraction waves.

Figures 12a to 12d show the variation with wavelength λ of the differences between the values of the normalized amplitudes $A_{j\alpha}$ for four oscillation modes for the DE1006, using the exact and long wavelength approximation of the Kochin function. The three values of wavelength considered in each figure correspond to ratioes $\lambda/B = 1.0$, 3.8, and 9.1. As expected, agreement is poor at $\lambda/B = 1.0$. However, there is only a slight difference at $\lambda/B = 3.8$, and nearly identical agreement at $\lambda/B = 9.1$. At the shortest wavelength, $\lambda/B = 1.0$, the agreement is better for the lateral modes of sway and yaw than for the vertical modes of heave and pitch. This is due to the fact that the long wavelength approximation in Eq. (7b) is accurate to second order in θ for the lateral modes, and only to first order for the vertical modes.

5. SUMMARY

The calculation procedure consists of two principal parts: the inner flow and far field regions. The inner flow near the hull is calculated by using the strip-theory Ship Motion Program. The principal output quantities of interest to the present work are the motion transfer coefficients and the singularity distribution over the hull surface. The far field ship radiation and diffraction wave patterns are obtained by using the Kochin function, which represents a weighted integral of the singularity distribution over the hull surface, in conjunction with an asymptotic expression for the waves due to an oscillating three-dimensional source. It is shown that a previously suggested approach of collapsing the hull surface singularity distribution to a line is equivalent to a long wavelength approximation of the Kochin function.

Wave patterns were calculated for six ship hulls, ranging in length from 140 to 990 ft. Four wavelengths of the exciting waves were used, ranging from 35 to 998 ft. Five wave headings were considered, ranging from following to head seas.

Among the six radiation modes, the waves due to surge tend to be an order of magnitude smaller than those of the other modes. Heave tends to give the largest wave amplitudes. The wave amplitudes due to surge, pitch, and yaw tend to have their minimum values in the beam direction, $\theta = 90$ deg., while the remaining three modes have their maximum values here. The major features of the long wavelength wave pattern are established for wavelengths of the exciting wave equal to one ship length.

The direction of the maxima of both the vertical (symmetrical) and lateral (antisymmetrical) components of the diffraction wave coincides with that of the wave heading β. The amplitudes of the vertical component do not vary with β while those of the lateral component are scaled by the factor $\sin \beta$.

The wave amplitudes calculated by using the long wavelength approximation and exact evaluation of the Kochin function are in poor agreement for wavelength-to-beam ratio λ/B of 1.0 but is in excellent agreement at $\lambda/B = 3.8$. At low values of λ/B, the approximation is more accurate for the lateral modes.

Due to its substantially larger draft-to-beam ratio, there is usually a striking difference between the wave patterns of the strut-like SHSTNA hull and the conventional ship hulls of comparable length. The amplitudes of this hull for all the lateral modes are typically one order of magnitude larger than those of the other hulls, while the vertical component of the diffraction wave is usually much smaller. The case of the vertical radiation waves is more complex. They may be much smaller (due to the narrow beam), or they may be somewhat larger than those of the other hulls (due to large amplitudes of oscillation near resonance, caused by small potential wave damping.)

6. REFERENCES

1. Salvesen, N., Tuck, E.O., and Faltinsen, O., "Ship Motions and Sea Loads," *Transactions of the Society of Naval Architects and Marine Engineers*, Vol. 78, pp. 250-287, November 1970.

2. Meyers, W.G., Applebee, T.R., and Baitis, A.E., "User's Manual for the Standard Ship Motion Program, SMP," DTNSRDC Report SPD-0936-01, September 1981.

3. Chang, M.S., "Computations of Three-Dimensional Ship-Motions with Forward Speed," *Proceedings of the Second International Conference on Numerical Ship Hydrodynamics*, pp. 124-135, September 1977.

4. Wang, H.T. and Chang, M.S., " Comparison of Force and Motion Predictions Using Strip Theory and a Three-Dimensional Method for Hulls at Zero Speed in Waves," DTNSRDC Report 82/025, June 1982.

5. Lee, C.M., O'Dea, J.F., and Meyers, W.G., "Prediction of Relative Motion of Ships in Waves," *Fourteenth Symposium on Naval Hydrodynamics*, pp. 417-452, August 1982.

6. Beck, R.F., "Relative Motion Components for a Mathematical Form in Regular Waves," *Fourteenth Symposium on Naval Hydrodynamics*, pp. 453-505, August 1982.

7. Newman, J.N., *Marine Hydrodynamics*, MIT Press, Cambridge, Massachusetts, 1978.

8. Wang, H.T., "Calculation of Far Field, Ship Radiation and Diffraction Waves," NRL Memorandum Report 5028, March 1983.

9. Frank, W., "Oscillation of Cylinders in or Below the Free Surface of Deep Fluids," NSRDC Report 2375, October 1967.

10. Wehausen, J.V. and Laitone, E.V., "Surface Waves," *Encyclopedia of Physics*, Vol. 9, Springer-Verlag, Berlin, pp. 446-778, 1960.

11. Marnyanskii, I.A., "Diffraction of Waves Around a Submerged Vertical Plate," *Prikladnaya Matematika i Mekhanika*, Vol. 18, No. 2, pp. 233-238, 1954 (in Russian).

12. Liu, H.C., "Uber die Entstehung von Ringwellen an einer Flüssigkeitsoberfläche durch unter dieser gelegene, kugelige periodische Quellensysteme," *Zeitschrift für Angewandte Mathematik und M chanik*, Vol. 32, No. 7, pp. 211-226, July 1952.

13. Sharma, S.D., "Some Results Concerning the Wavemaking of a Thin Ship," *Journal of Ship Research*, Vol. 13, No. 1, pp. 72-81, March 1969.

14. Lee, C.M., "Theoretical Prediction of Motion of Small-Waterplane-Area, Twin-Hull (SWATH) Ships in Waves," DTNSRDC Report 76-0046, December 1970.

Table 1—Summary of Hull Geometric Characteristics

Ship Hull	L (ft)	B/L	D/L	Appendages
1. DE1006	308	.117	.039	Yes
2. DE10NA	308	.117	.039	No
3. CVA59	990	.131	.036	Yes
4. CVASH	308	.131	.036	Yes
5. CVAXS	140	.131	.036	Yes
6. SHSTNA	308	.050	.150	No

L = length, B = beam, D = draft

Table 2—Summary of Exciting Wave Characteristics

Sea State No.	Wavelength λ (ft)	Frequency ω (rad/s)	Amplitude α (ft)
2	35.1	2.40	1.0
4	140.4	1.20	3.6
6	315.9	0.80	8.2
8	998.3	0.45	22.8

14

ξ_1 = SURGE ξ_3 = HEAVE ξ_5 = PITCH
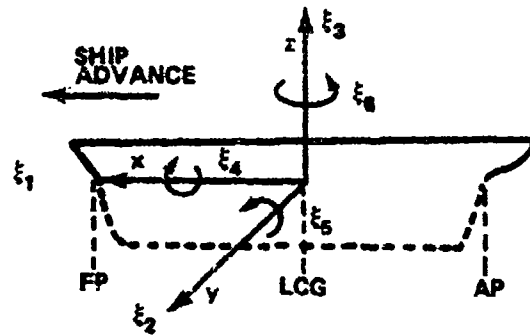
ξ_2 = SWAY ξ_4 = ROLL ξ_6 = YAW

Fig. 1 — Definition of coordinate system and six modes of ship oscillation
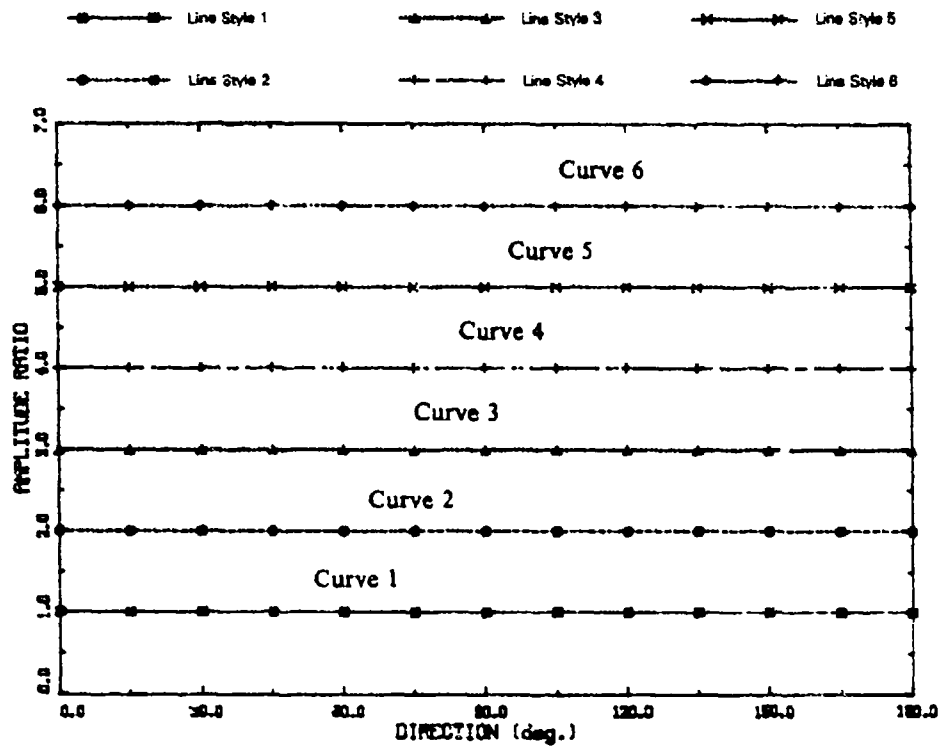
Fig. 2 — Definition of curve line styles
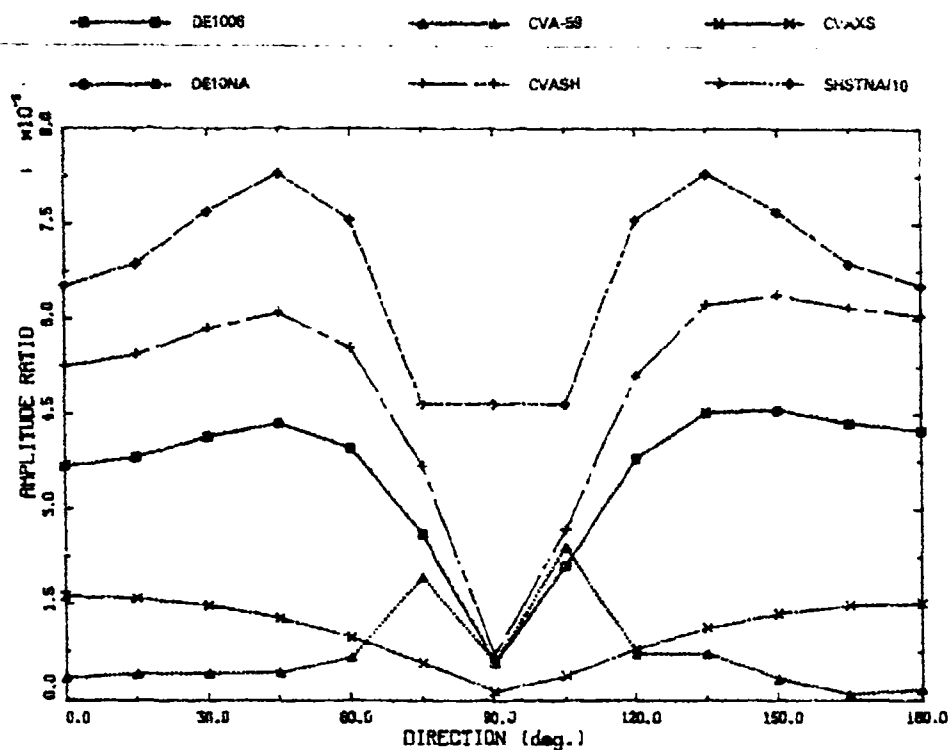
(a) $j = 1$, surge, $\lambda = 315.9$ ft, $\beta = 135$ deg
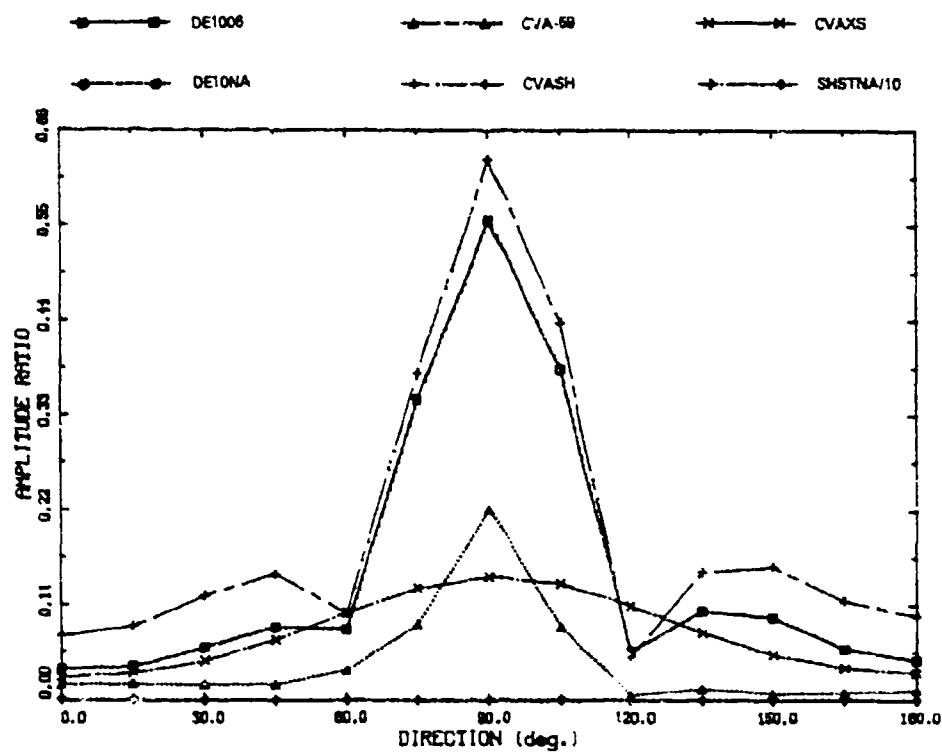
(b) $j = 3$, heave, $\lambda = 140.4$ ft, $\beta = 90$ deg

Fig. 3 — Dimensionless amplitude coefficient $A_{j\alpha}$ for radiation modes for all six hulls
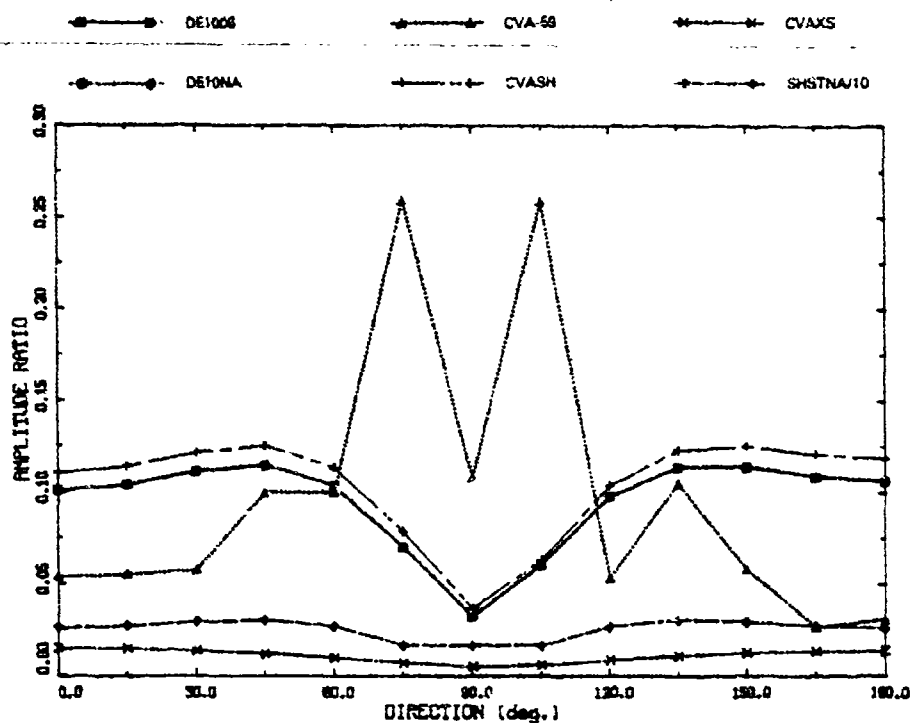
(c) $j = 5$, pitch, $\lambda = 315.9$ ft, $\beta = 135$ deg
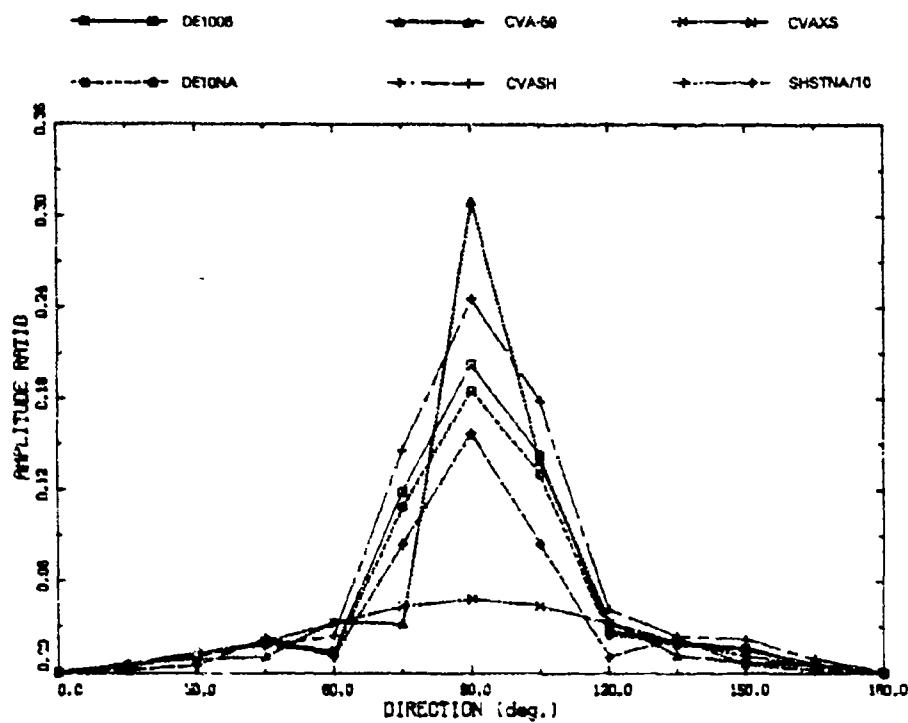
(d) $j = 2$, sway, $\lambda = 140.4$ ft, $\beta = 90$ deg

Fig. 3 (Continued) — Dimensionless amplitude coefficient $A_{j\alpha}$ for radiation modes for all six hulls
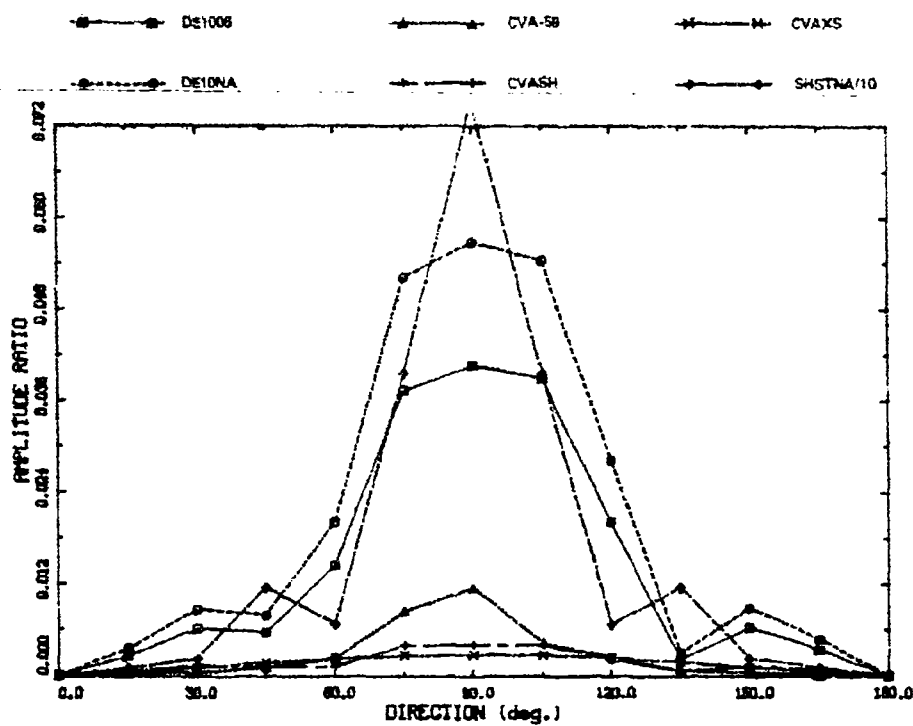
(e) $j = 4$, roll, $\lambda = 140.4$ ft, $\beta = 90$ deg
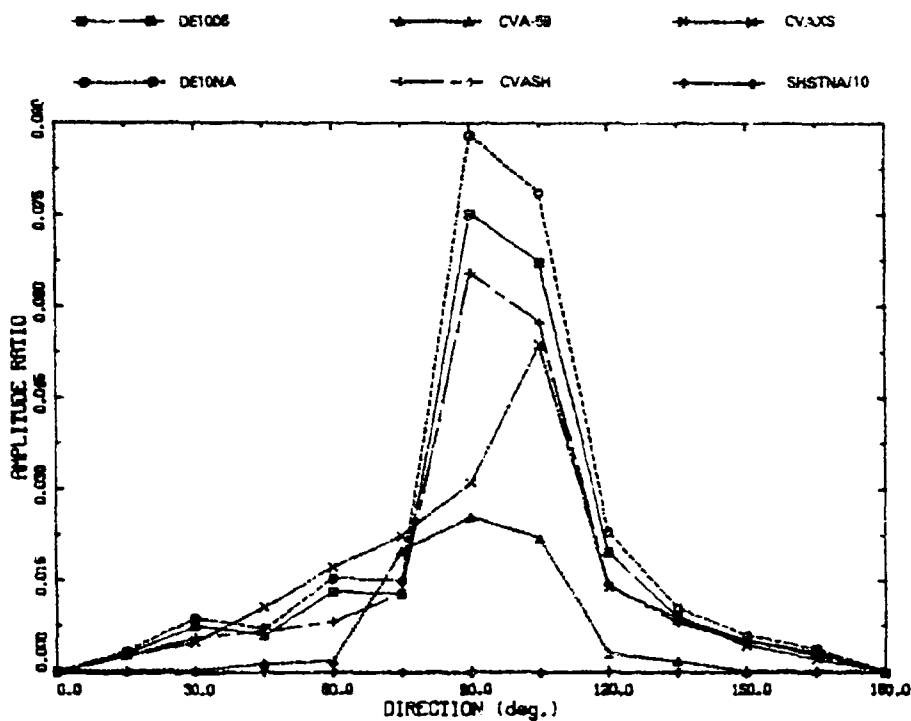
(f) $j = 6$, yaw, $\lambda = 35.1$ ft, $\beta = 90$ deg

Fig. 3 (Continued) — Dimensionless amplitude coefficient $A_{j\alpha}$ for radiation modes for all six hulls

18
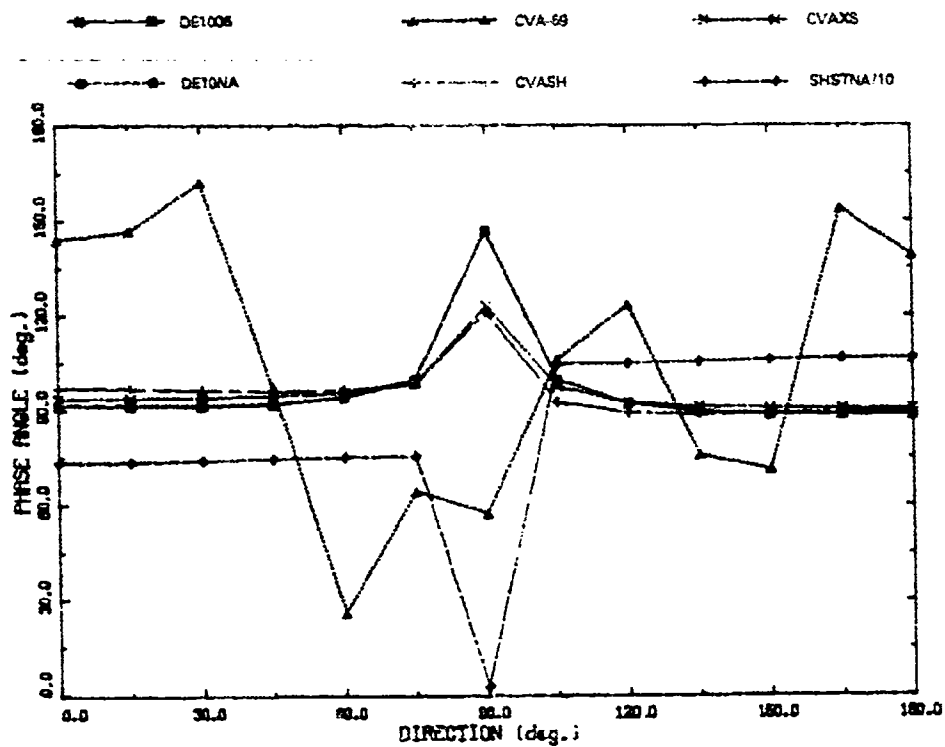
(a) $j = 1$, surge, $\lambda = 315.9$ ft, $\beta = 135$ deg
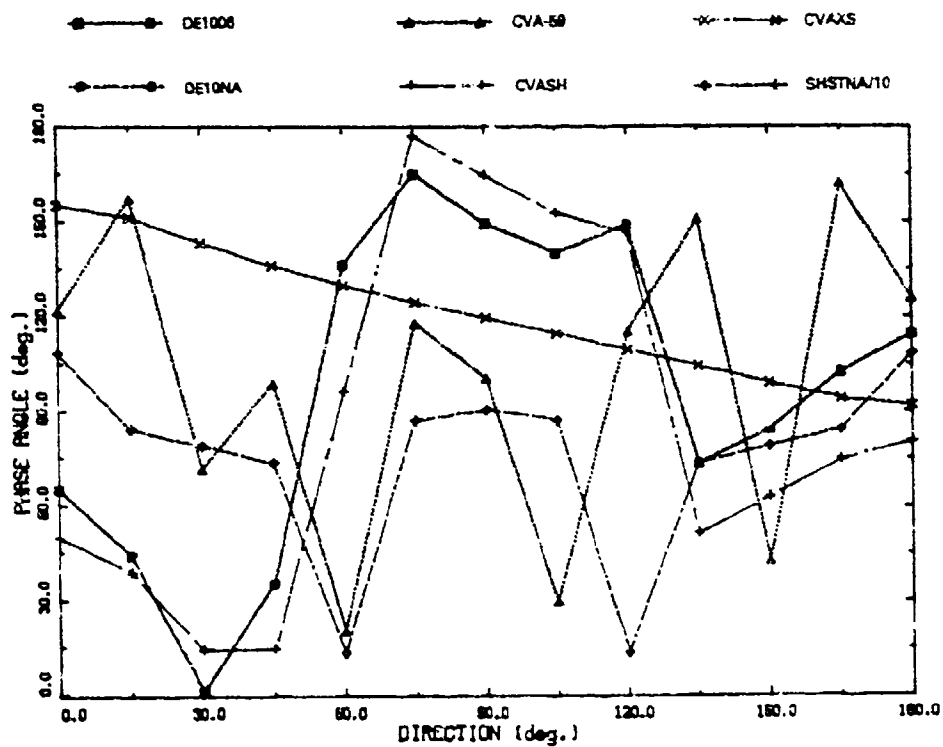
(b) $j = 3$, heave, $\lambda = 140.4$ ft, $\beta = 90$ deg

Fig. 4 — Phase angle ψ_j for radiation modes for all six hulls
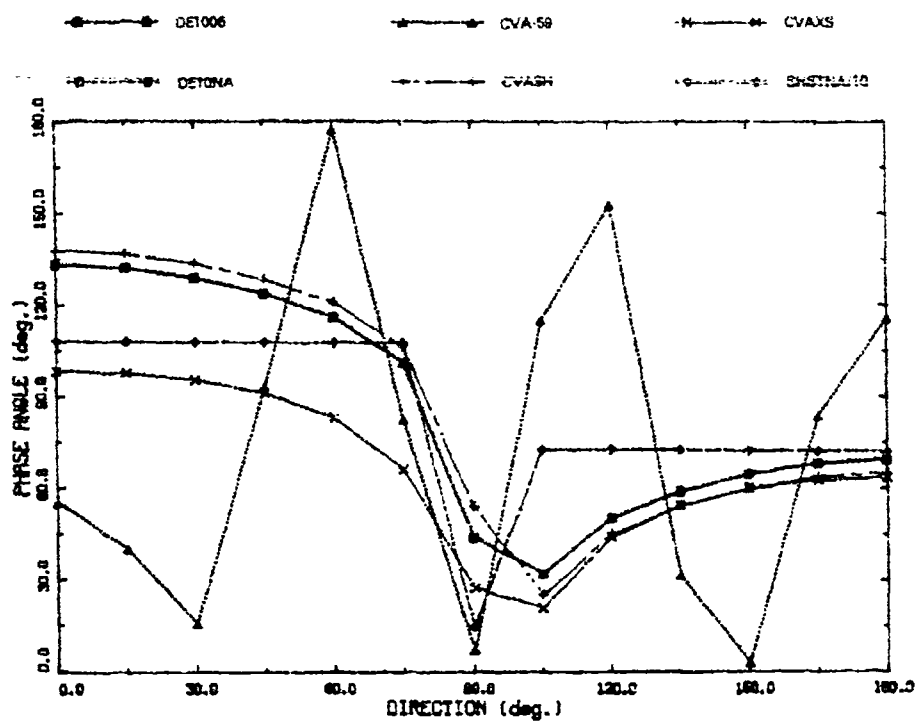
(c) $j = 5$, pitch, $\lambda = 315.9$ ft, $\beta = 135$ deg
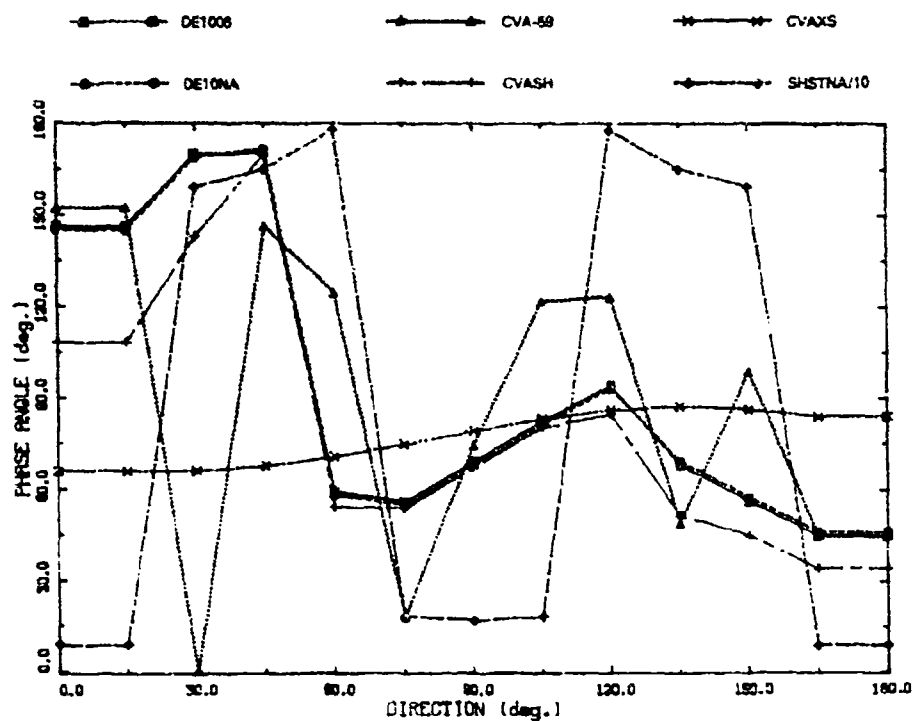
(d) $j = 2$, sway, $\lambda = 140.4$ ft, $\beta = 90$ deg

Fig. 4 (Continued) — Phase angle ψ_j for radiation modes for all six hulls
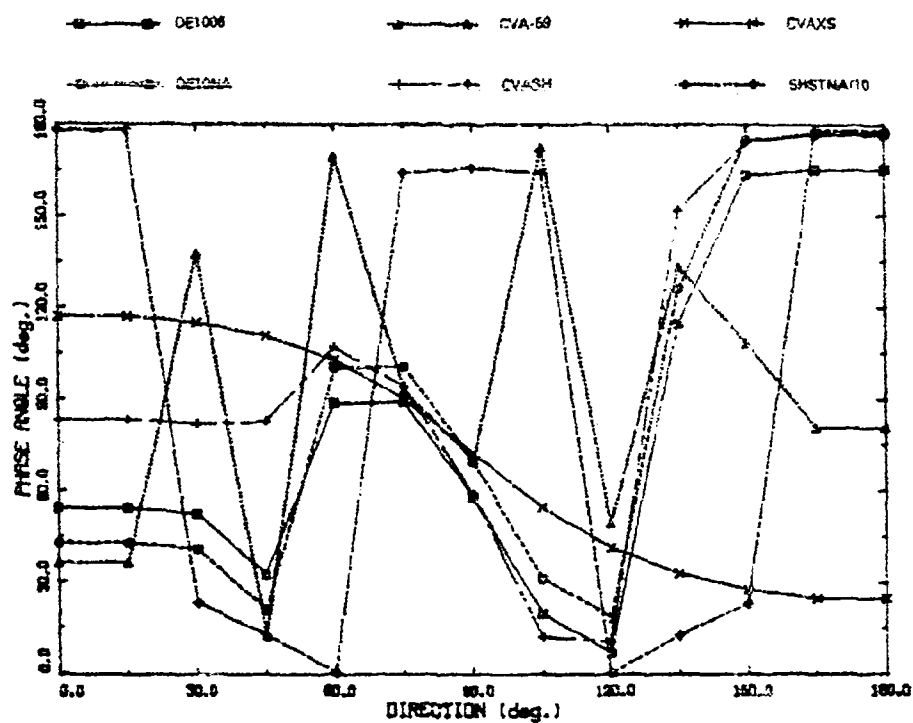
(e) $j = 4$, roll, $\lambda = 140.4$ ft, $\beta = 90$ deg
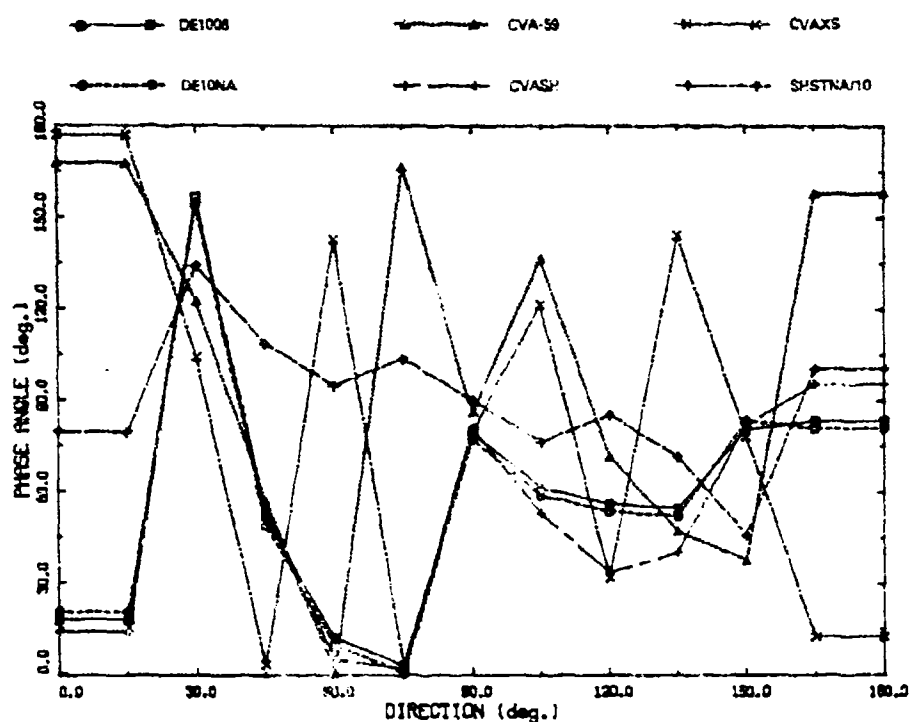
(f) $j = 6$, yaw, $\lambda = 35.1$ ft, $\beta = 90$ deg

Fig. 4 (Continued) — Phase angle ψ_j for radiation modes for all six hulls
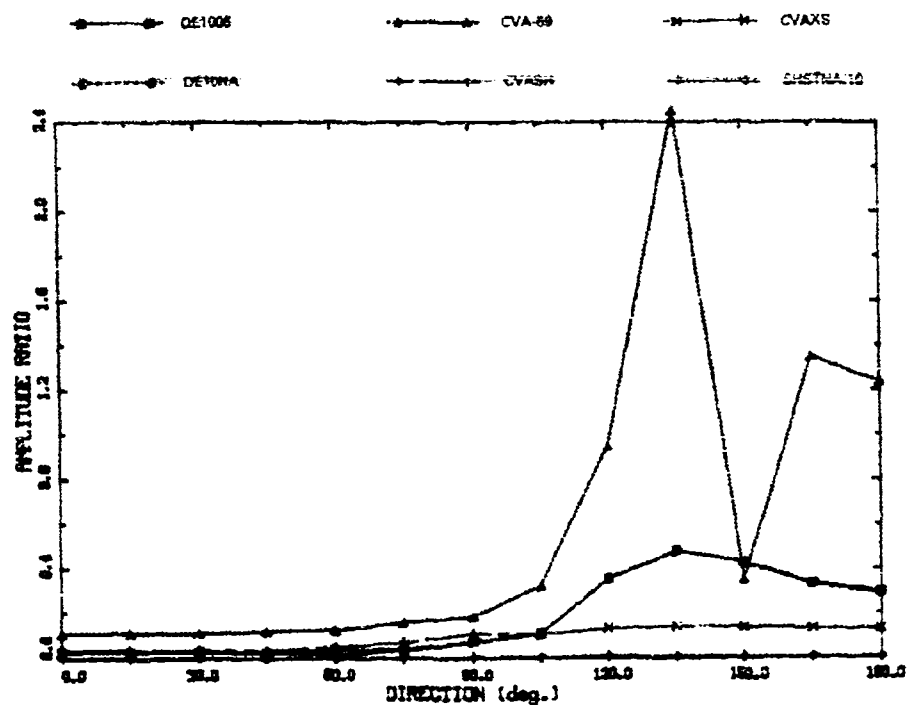
(a) A_{7V_a}, $\lambda = 140.4$ ft, $\beta = 135$ deg
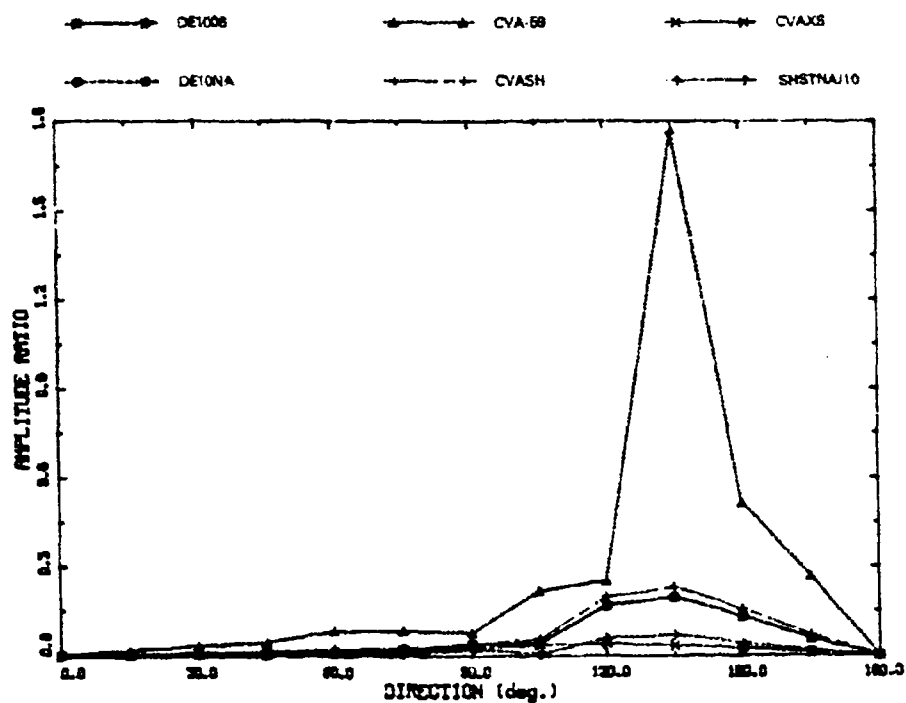
(b) A_{7L_a}, $\lambda = 140.4$ ft, $\beta = 135$ deg

Fig. 5 — Dimensionless amplitude coefficients A_{7V_a} and A_{7L_a} for diffraction wave for all six hulls

22

(a) ψ_{7V}, $\lambda = 140.4$ ft, $\beta = 135$ deg

(b) ψ_{7L}, $\lambda = 140.4$ ft, $\beta = 135$ deg
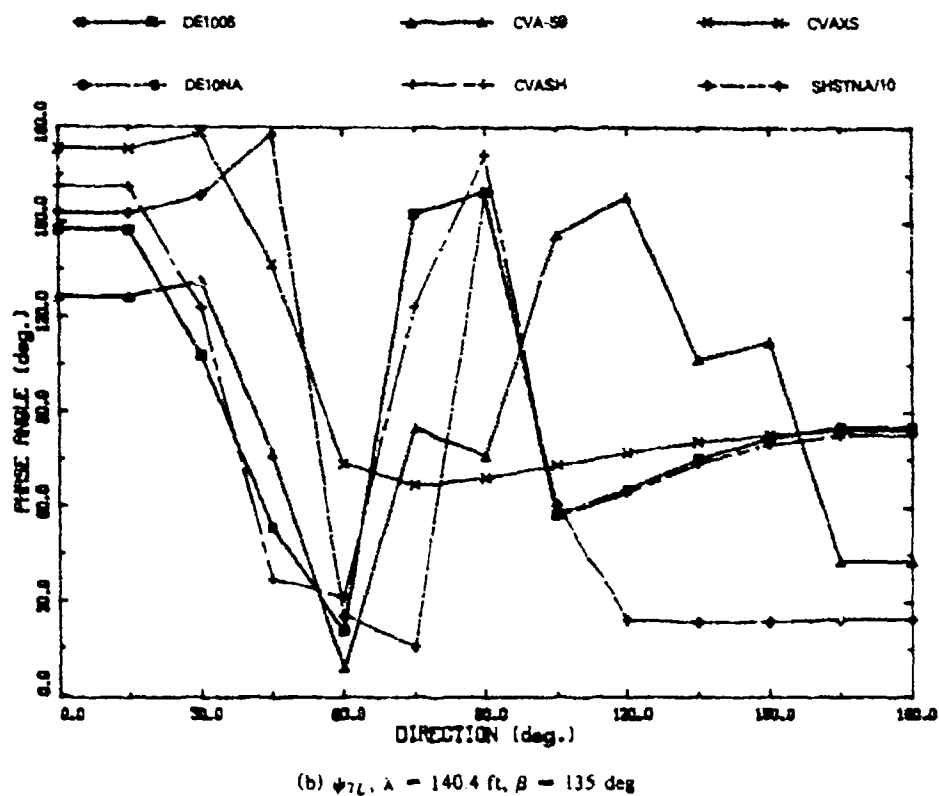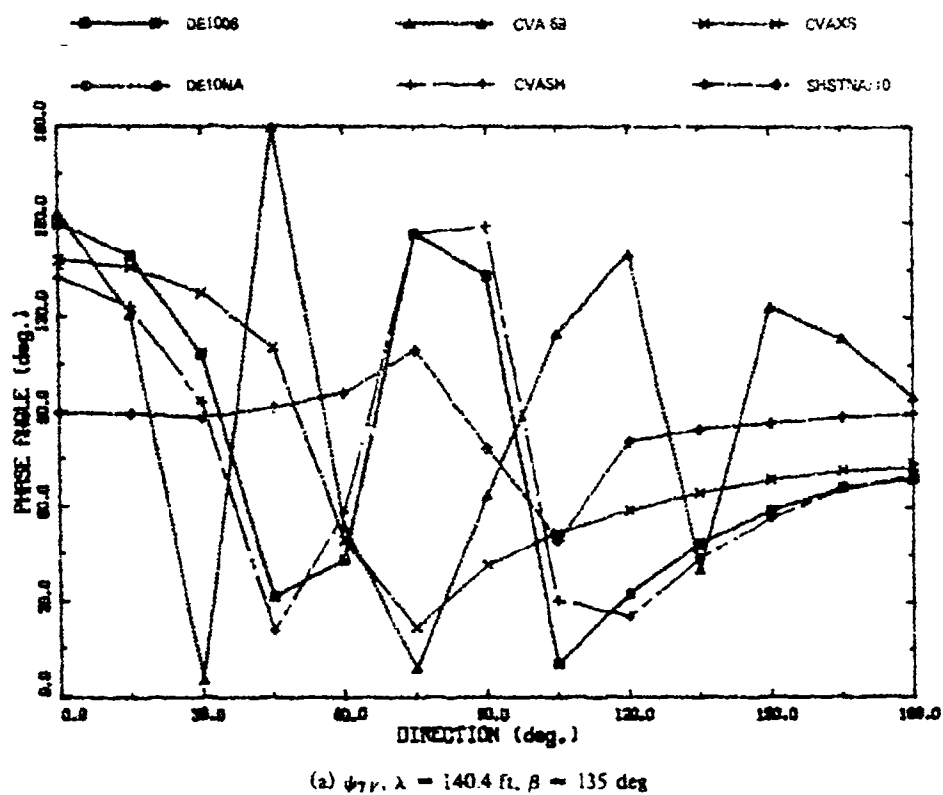
Fig. 6 — Phase angles ψ_{7V} and ψ_{7L} for diffraction wave for all six hulls

23
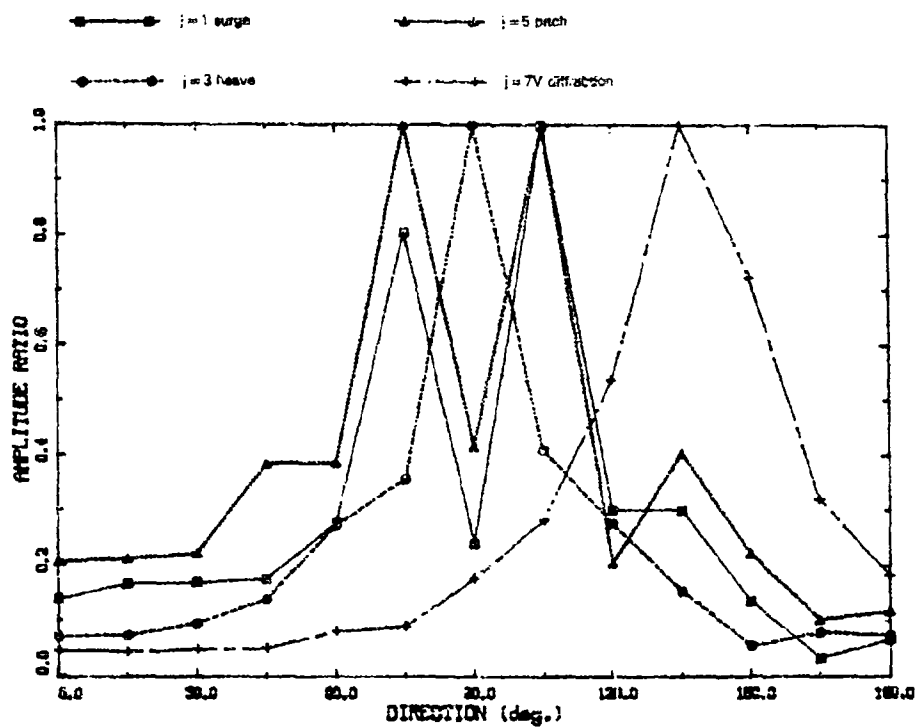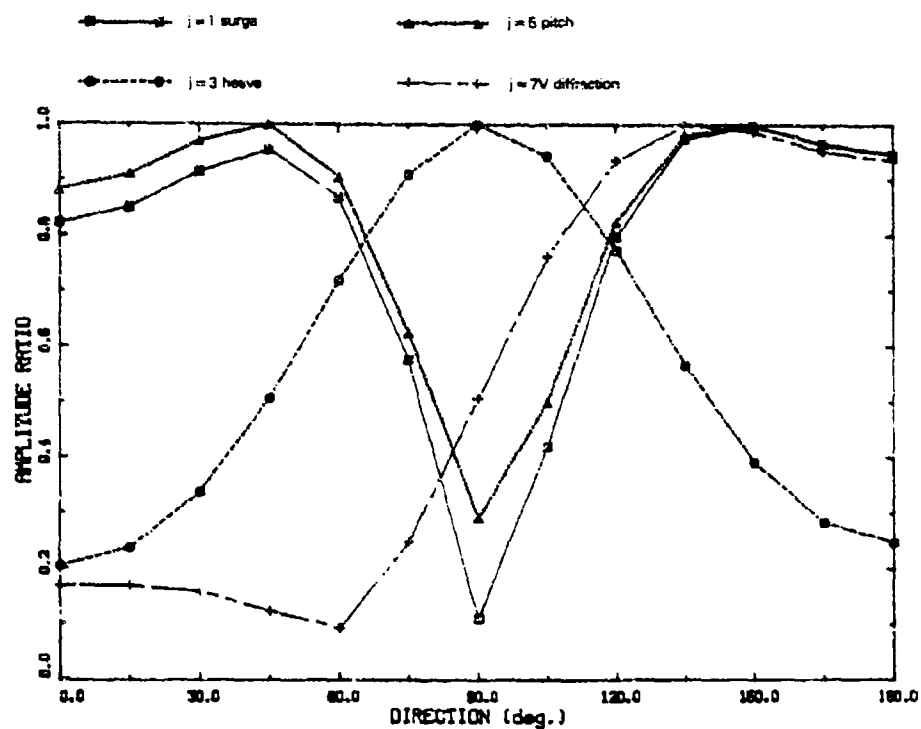
(a) CVA-59

(b) CVASH

Fig. 7 — Normalized amplitude coefficient A_{j8} for the vertical modes for CVA-59, CVASH, and CVAXS, $\lambda = 315.9$ ft, $\beta = 135$ deg
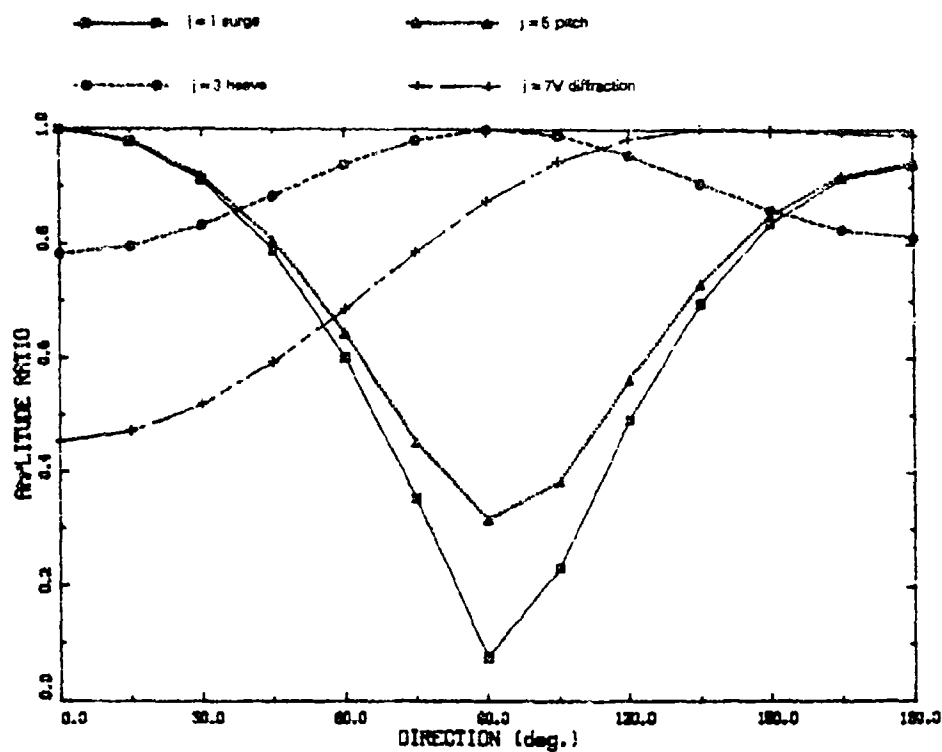
(c) CVAXS

Fig. 7 (Continued) — Normalized amplitude coefficient A_{j8} for the vertical modes for CVA-59, CVASH, and CVAXS, $\lambda = 315.9$ ft, $\beta = 135$ deg
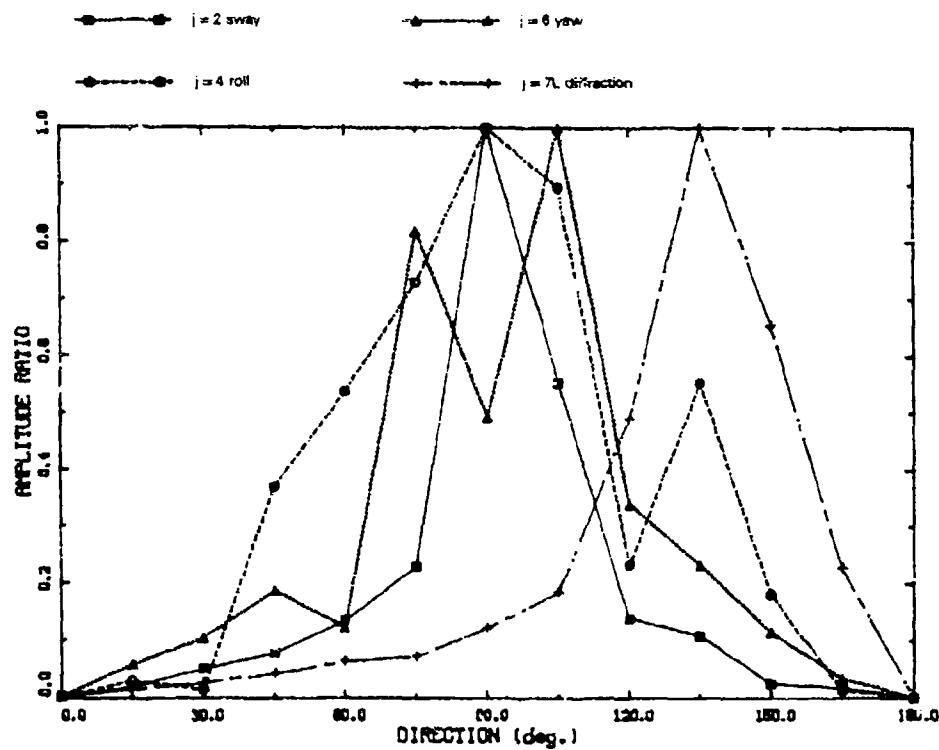
(a) CVA-59

Fig. 8 — Normalized amplitude coefficient A_{j8} for the lateral modes for CVA-59, CVASH, and CVAXS, $\lambda = 315.9$ ft, $\beta = 135$ deg

25
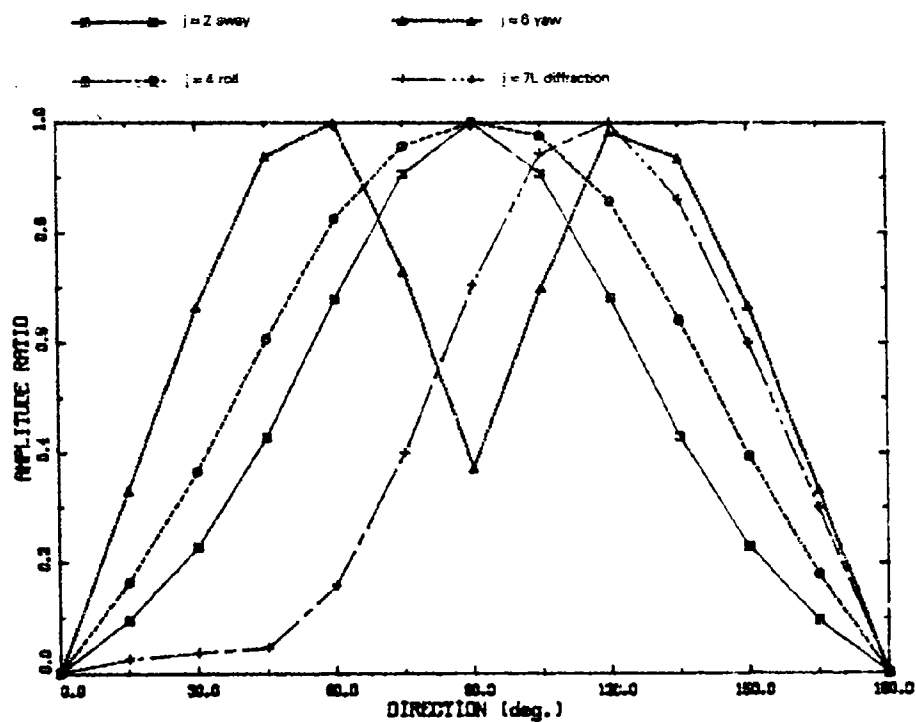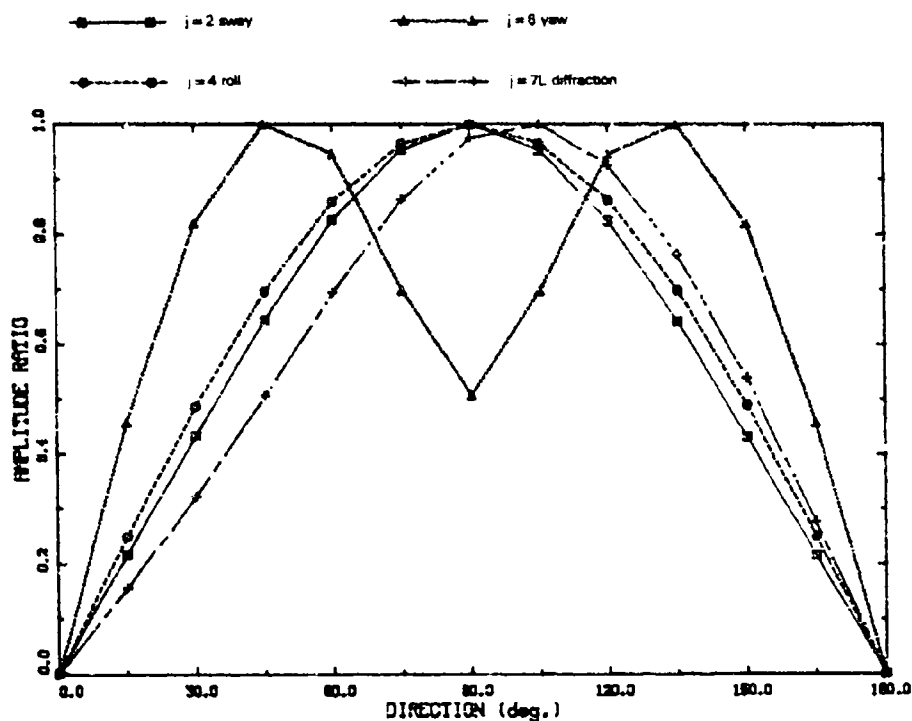
(b) CVASH

(c) CVAXS

Fig. 8 (Continued) — Normalized amplitude coefficient A_{ij} for the lateral modes
for CVA-59, CVASH, and CVAXS, $\lambda = 315.9$ ft, $\beta = 135$ deg
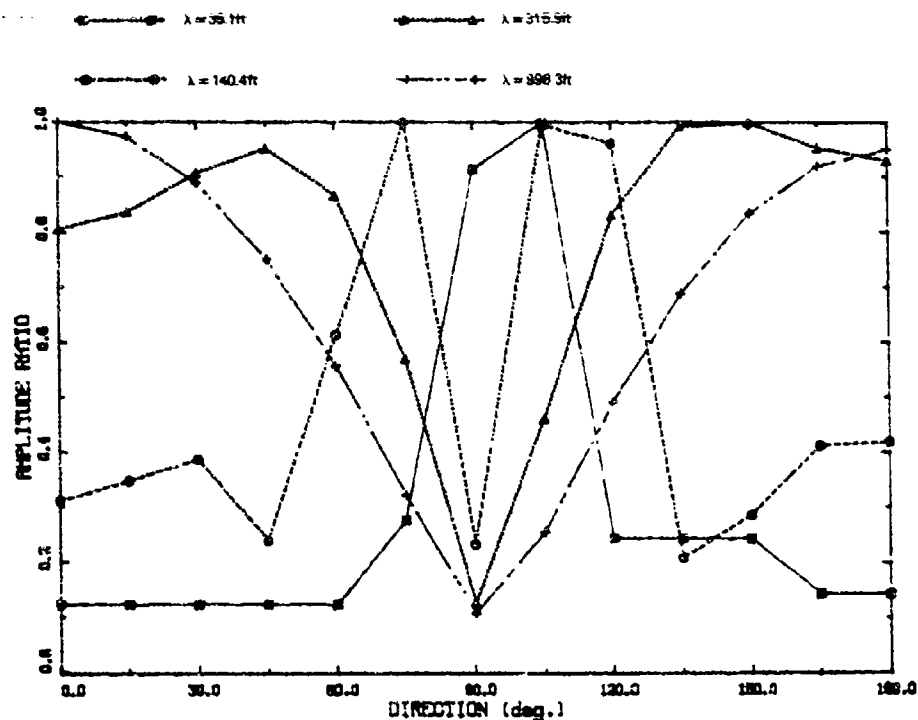
(a) $j = 1$, surge, $\beta = 135$ deg
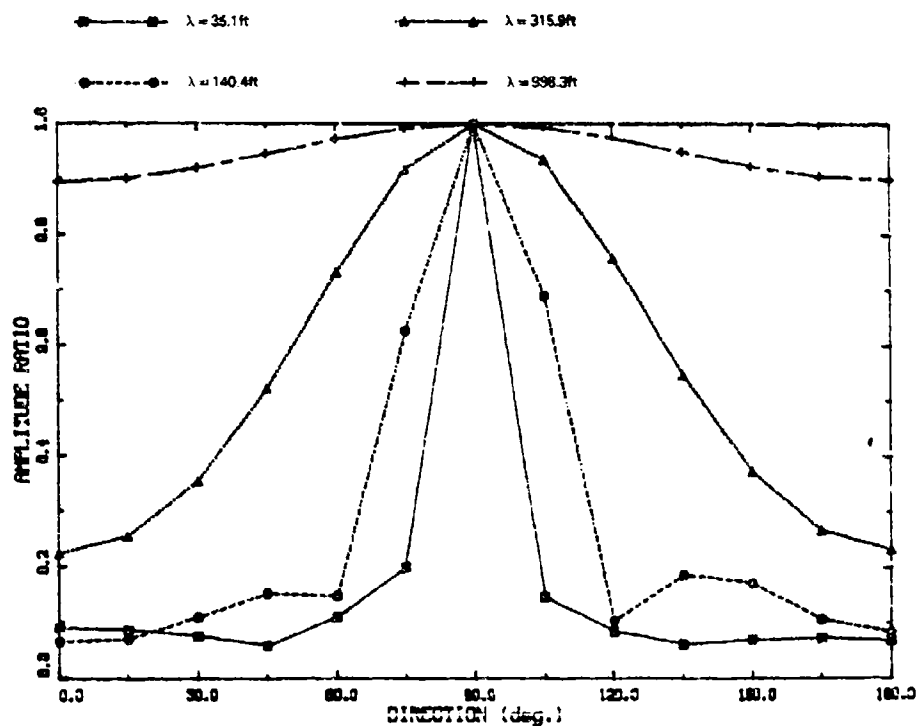
(b) $j = 3$, heave, $\beta = 90$ deg

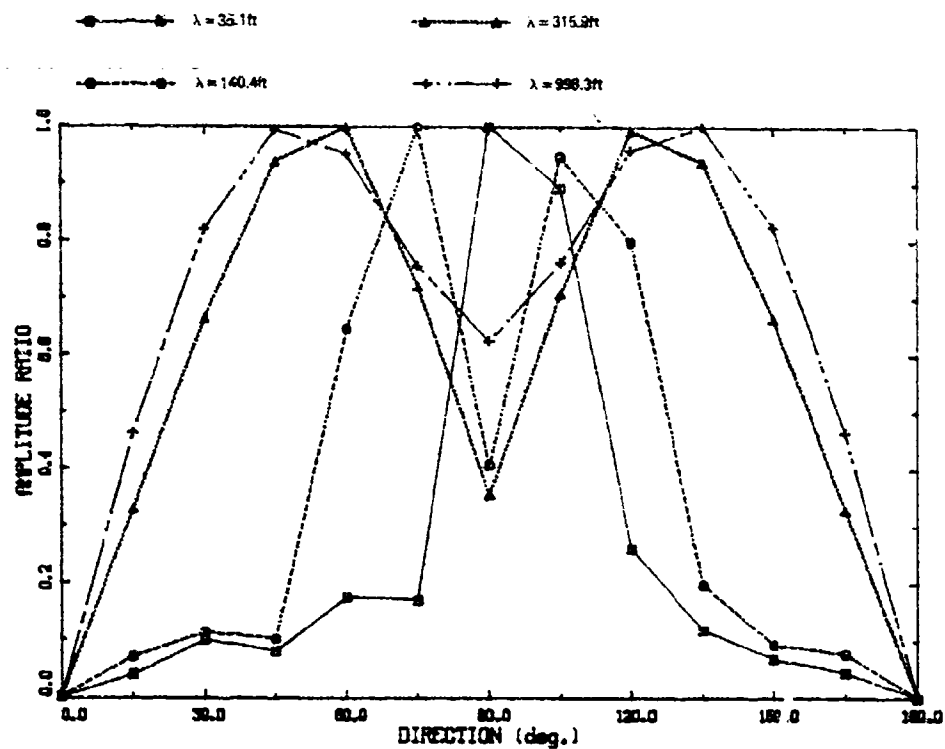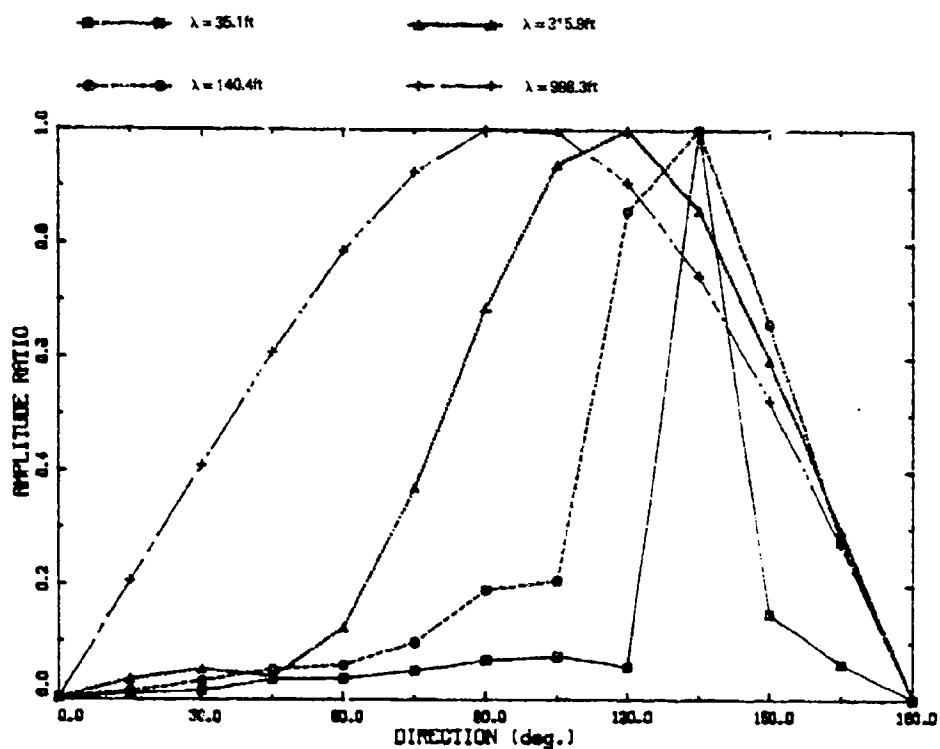Fig. 9 — Normalized amplitude coefficient $A_{j\delta}$ for the vertical modes of the DE1006 for different wavelengths
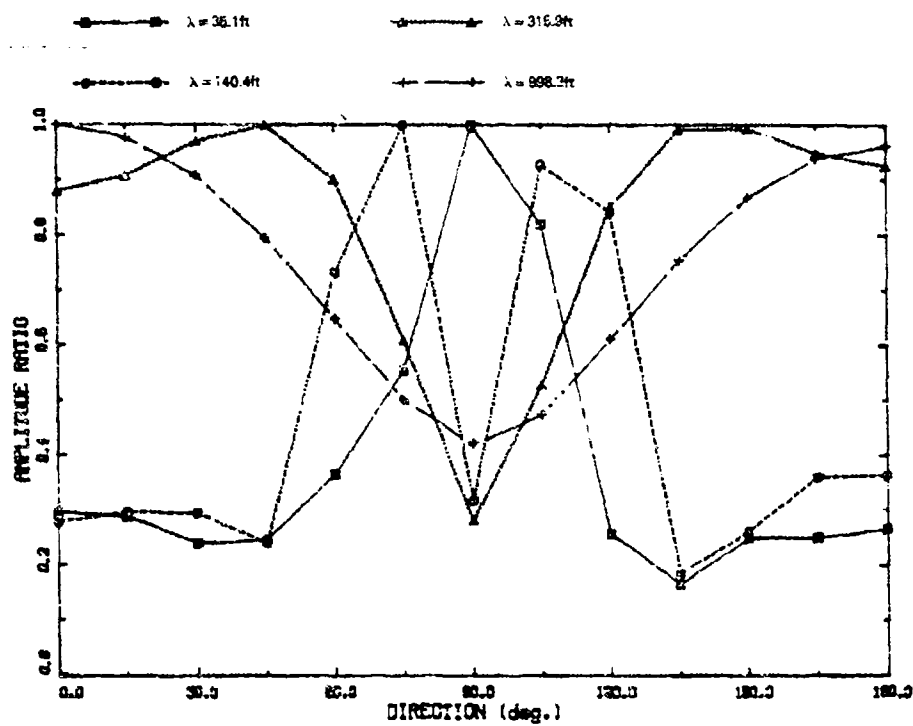
(c) $j = 5$, pitch, $\beta = 135$ deg
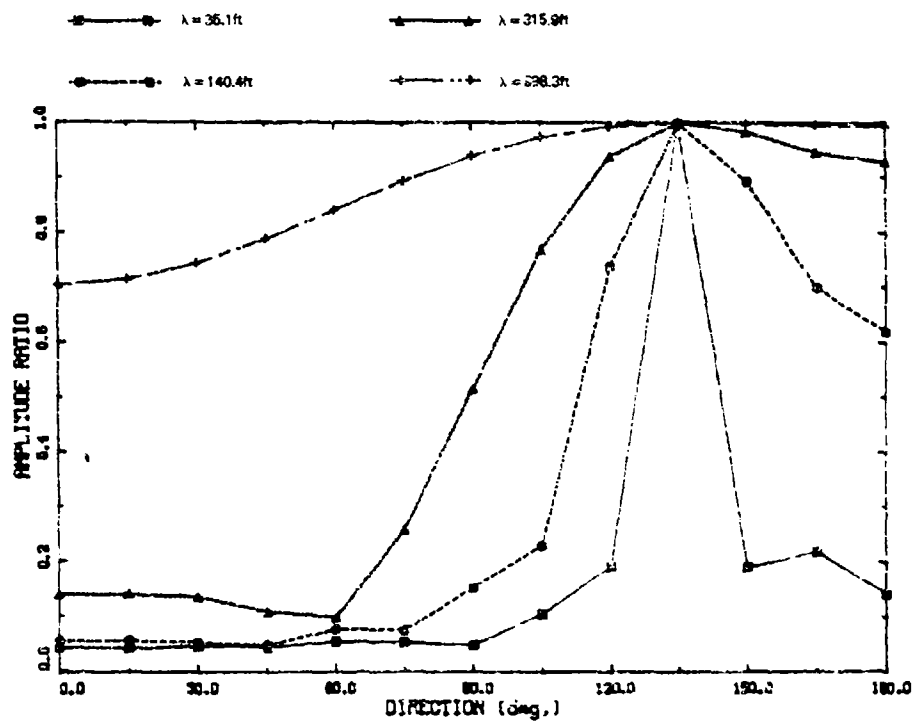
(d) $j = 7V$, diffraction, $\beta = 135$ deg

Fig. 9 (Continued) — Normalized amplitude coefficient $A_{j\delta}$ for the vertical modes of the DF1006 for different wavelengths
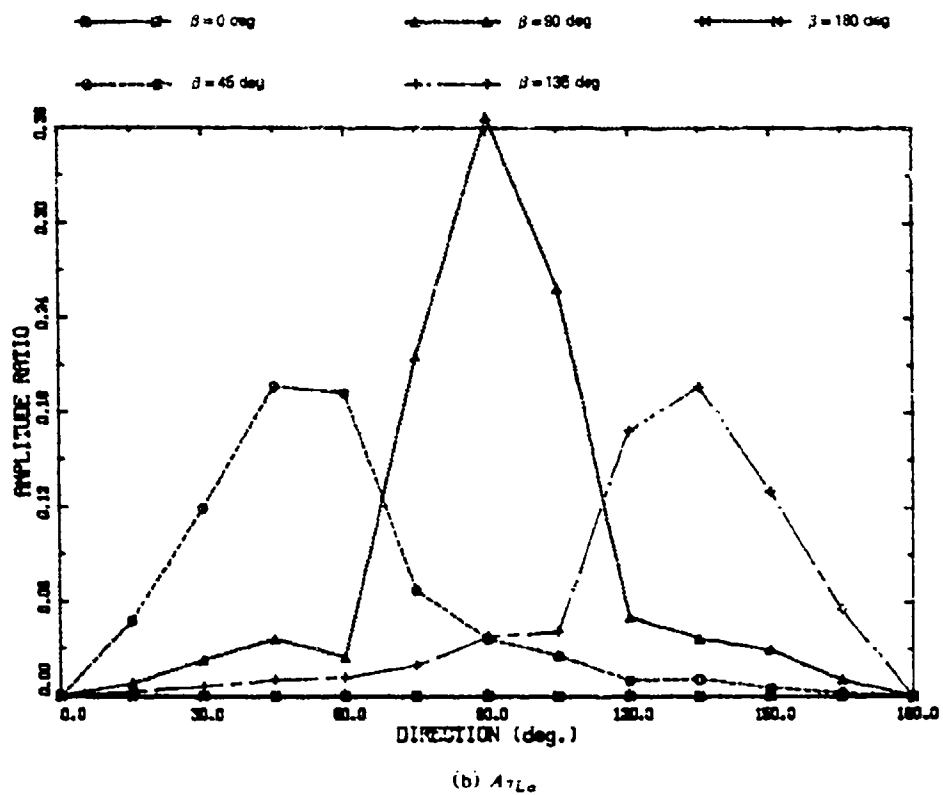
28
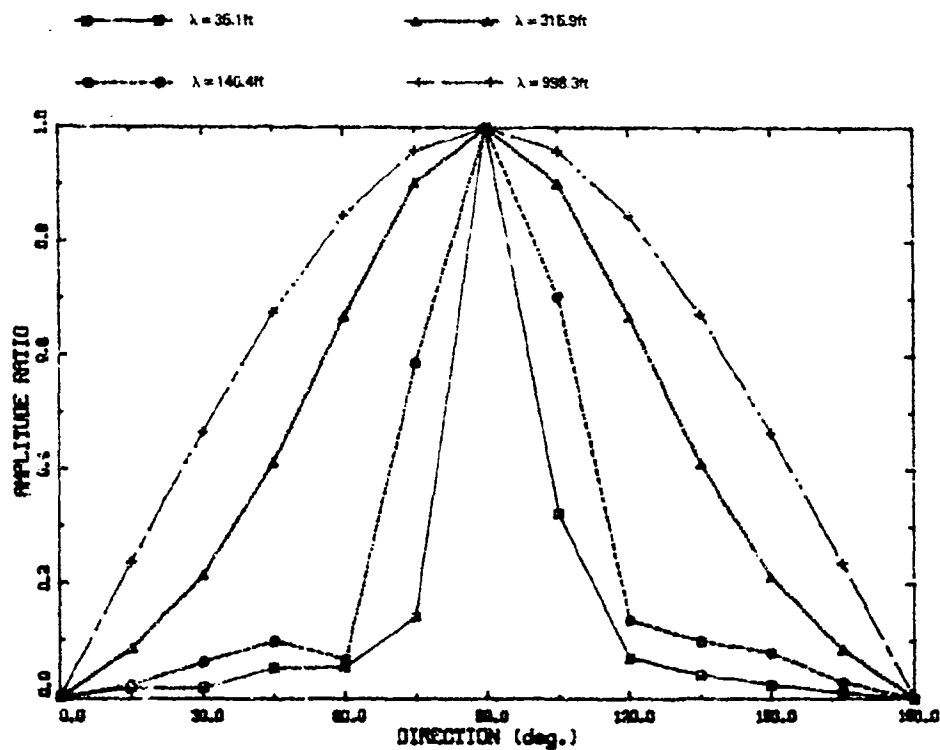
(a) $j = 2$, sway, $\beta = 90$ deg
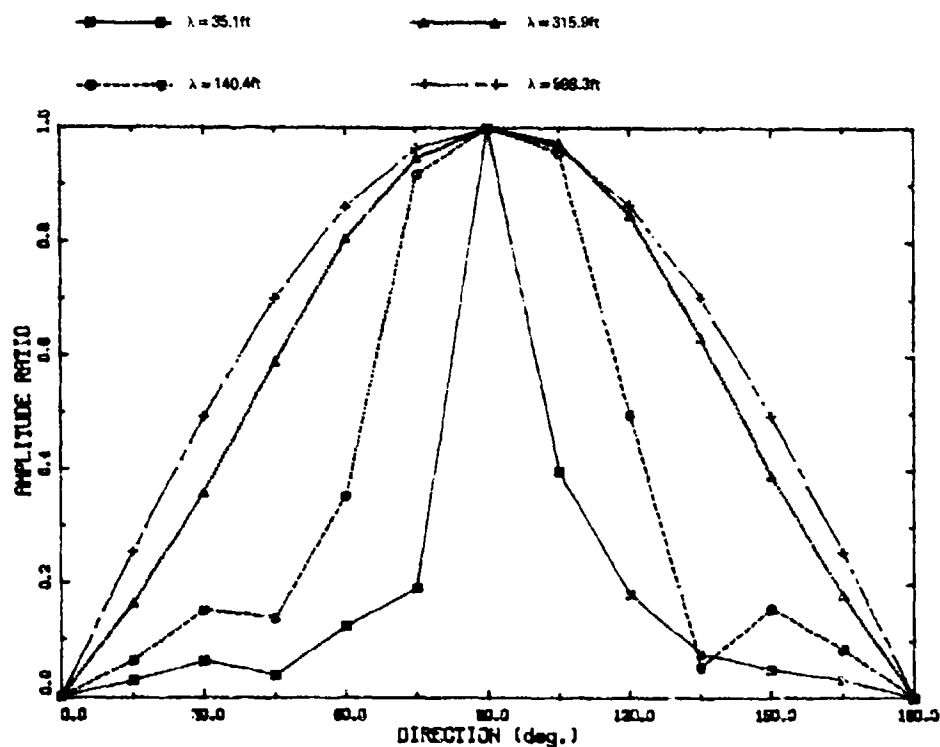
(b) $j = 4$, roll, $\beta = 90$ deg

Fig. 10 — Normalized amplitude coefficient $A_{j\delta}$ for the lateral modes of the DE1006 for different wavelengths

(c) $j = 6$, yaw, $\beta = 45$ deg

(d) $j = 7L$, diffraction, $\beta = 135$ deg

Fig. 10 (Continued) — Normalized amplitude coefficient $A_{j\delta}$ for the lateral modes of the DE1006 for different wavelengths
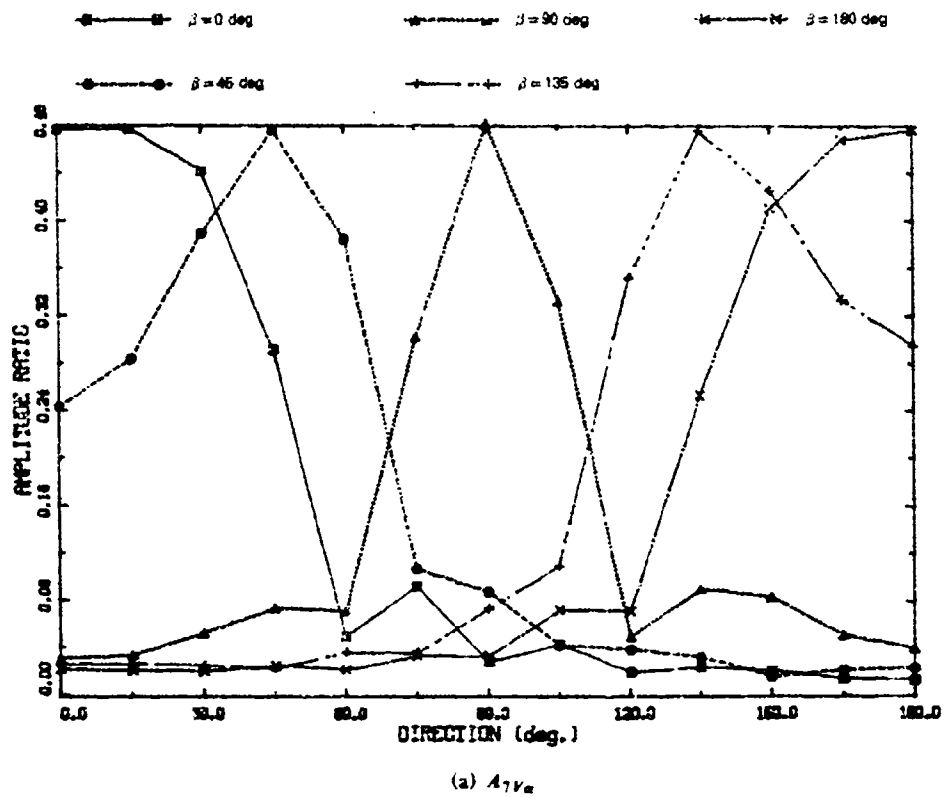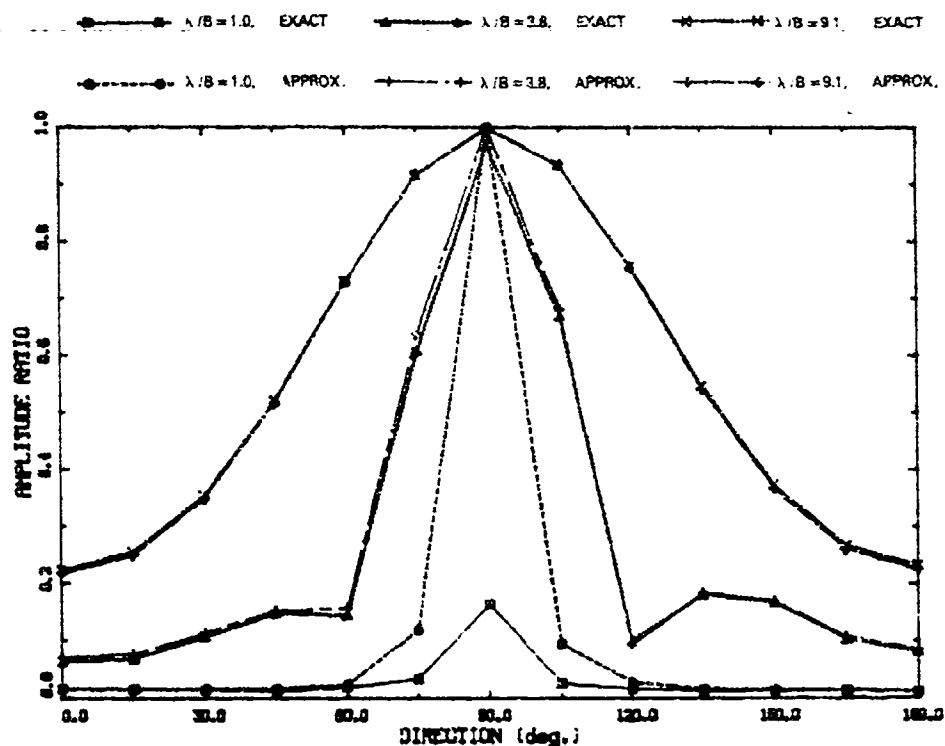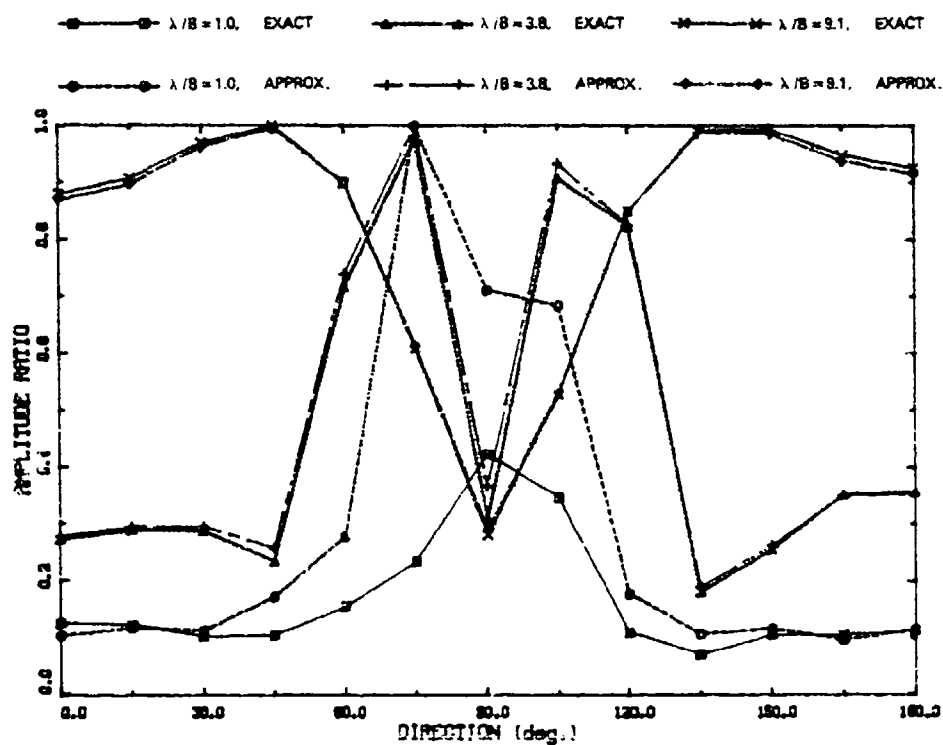
(a) A_{7V_α}

(b) A_{7L_α}

Fig. 11 — Dimensionless amplitude coefficients A_{7V_α} and A_{7L_α} for the diffraction wave of the DE1006 for different wave headings, $\lambda = 140.4$ ft

31

(a) $j = 3$, heave

(b) $j = 5$, pitch

Fig. 12 — Exact and approximate values of normalized amplitude coefficient $A_{j\epsilon}$
for four radiation modes of the DE1006 for different wavelengths, $\beta = 90$ deg
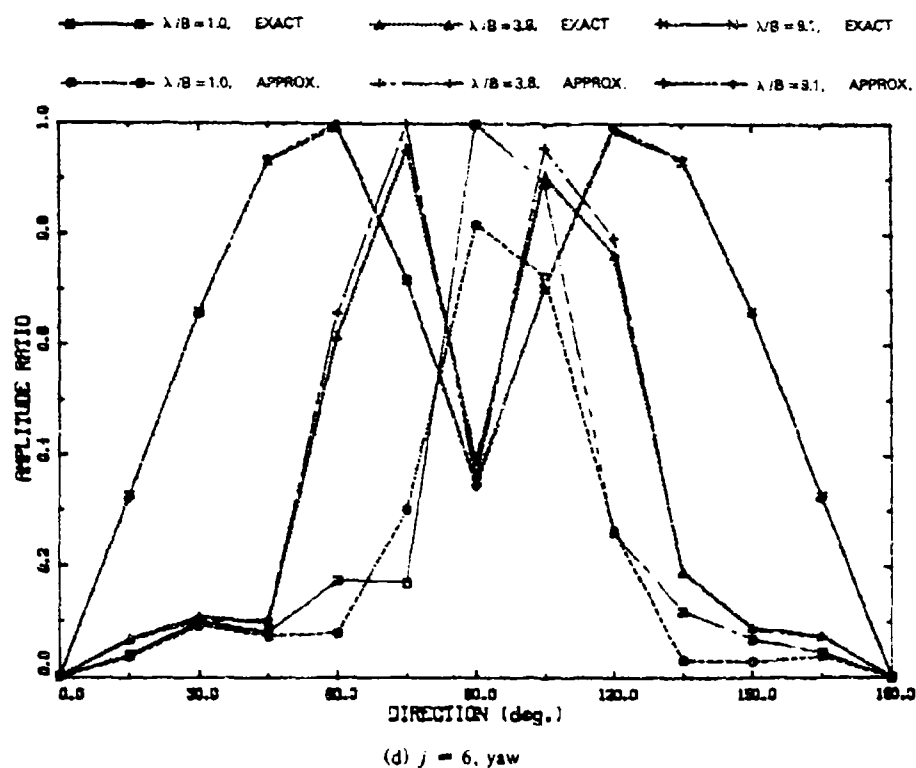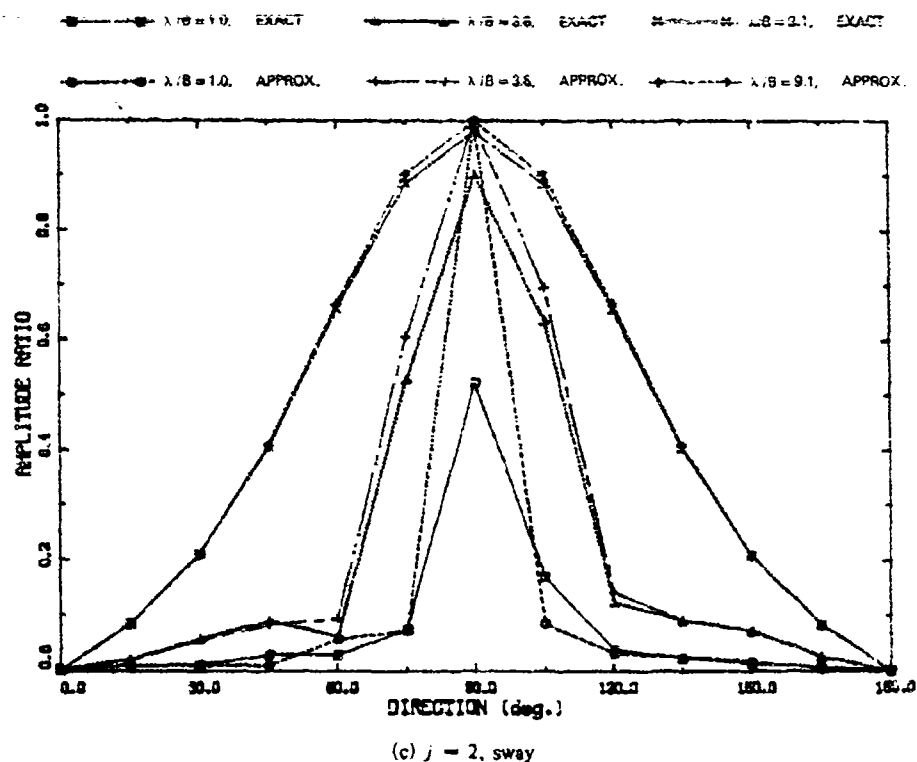
32

(c) $j = 2$, sway

(d) $j = 6$, yaw

Fig. 12 (Continued) — Exact and approximate values of normalized amplitude coefficient A_{j4} for four radiation modes of the DE1006 for different wavelengths, $\beta = 90$ deg